2019-06

OBSERVATIONS OF ENVIRONMENTAL FACTORS AFFECTING INTENSITY CHANGES DURING THE TRACK REVERSAL OF HURRICANE JOAQUIN (2015)

Buholzer, Natasha

Monterey, CA; Naval Postgraduate School

NAVAL POSTGRADUATE SCHOOL

MONTEREY, CALIFORNIA

THESIS

OBSERVATIONS OF ENVIRONMENTAL FACTORS AFFECTING INTENSITY CHANGES DURING THE TRACK REVERSAL OF HURRICANE JOAQUIN (2015)

by

Natasha Buholzer

June 2019

Thesis Advisor: Wendell A. Nuss
Co-Advisor: Russell L. Elsberry

THIS PAGE INTENTIONALLY LEFT BLANK

REPORT DOCUMENTATION PAGE	*Form Approved OMB No. 0704-0188*

1. AGENCY USE ONLY *(Leave blank)*	**2. REPORT DATE** June 2019	**3. REPORT TYPE AND DATES COVERED** Master's thesis

4. TITLE AND SUBTITLE OBSERVATIONS OF ENVIRONMENTAL FACTORS AFFECTING INTENSITY CHANGES DURING THE TRACK REVERSAL OF HURRICANE JOAQUIN (2015)	**5. FUNDING NUMBERS** NPSCA39435463
6. AUTHOR(S) Natasha Buholzer	
7. PERFORMING ORGANIZATION NAME(S) AND ADDRESS(ES) Naval Postgraduate School Monterey, CA 93943-5000	**8. PERFORMING ORGANIZATION REPORT NUMBER**
9. SPONSORING / MONITORING AGENCY NAME(S) AND ADDRESS(ES) N/A	**10. SPONSORING / MONITORING AGENCY REPORT NUMBER**

11. SUPPLEMENTARY NOTES The views expressed in this thesis are those of the author and do not reflect the official policy or position of the Department of Defense or the U.S. Government.

12a. DISTRIBUTION / AVAILABILITY STATEMENT Approved for public release. Distribution is unlimited.	**12b. DISTRIBUTION CODE** A

13. ABSTRACT (maximum 200 words)

The objective of this thesis is to better understand the environmental factors and internal processes that contributed to the unusual track reversal of Hurricane Joaquin (2015) north of the Bahamas and the two rapid intensification events. Special reprocessed Atmospheric Motion Vector (AMV) and Satellite Consensus (SATCON) datasets were used to document the vertical extent of the inner vortex convection and the outflow level and strength of Joaquin. The hypothesis of this study is the addition of high temporal and spatial resolution AMVs and SATCON data over the vortex and the surrounding environment will further explain the contributing factors to the track and intensity events of Joaquin. The Joaquin case well illustrates that the relationship between environmental VWS and tropical cyclone intensity change can be highly non-linear and that the ocean cooling contributed highly to Joaquin's intensification and decay.

14. SUBJECT TERMS tropical cyclone, hurricane, Joaquin, track, forecast, atmospheric motion vectors, intensity, ocean-cooling, non-linear correlation	**15. NUMBER OF PAGES** 75
	16. PRICE CODE

17. SECURITY CLASSIFICATION OF REPORT	**18. SECURITY CLASSIFICATION OF THIS PAGE**	**19. SECURITY CLASSIFICATION OF ABSTRACT**	**20. LIMITATION OF ABSTRACT**
Unclassified	Unclassified	Unclassified	UU

NSN 7540-01-280-5500 Standard Form 298 (Rev. 2-89) Prescribed by ANSI Std. 239-18

THIS PAGE INTENTIONALLY LEFT BLANK

Approved for public release. Distribution is unlimited.

OBSERVATIONS OF ENVIRONMENTAL FACTORS AFFECTING INTENSITY CHANGES DURING THE TRACK REVERSAL OF HURRICANE JOAQUIN (2015)

Natasha Buholzer
Lieutenant, United States Navy
BS, U.S. Naval Academy, 2010

Submitted in partial fulfillment of the
requirements for the degree of

MASTER OF SCIENCE IN METEOROLOGY AND PHYSICAL OCEANOGRAPHY

from the

NAVAL POSTGRADUATE SCHOOL
June 2019

Approved by: Wendell A. Nuss
Advisor

Russell L. Elsberry
Co-Advisor

Wendell A. Nuss
Chair, Department of Meteorology

THIS PAGE INTENTIONALLY LEFT BLANK

ABSTRACT

The objective of this thesis is to better understand the environmental factors and internal processes that contributed to the unusual track reversal of Hurricane Joaquin (2015) north of the Bahamas and the two rapid intensification events. Special reprocessed Atmospheric Motion Vector (AMV) and Satellite Consensus (SATCON) datasets were used to document the vertical extent of the inner vortex convection and the outflow level and strength of Joaquin. The hypothesis of this study is the addition of high temporal and spatial resolution AMVs and SATCON data over the vortex and the surrounding environment will further explain the contributing factors to the track and intensity events of Joaquin. The Joaquin case well illustrates that the relationship between environmental VWS and tropical cyclone intensity change can be highly non-linear and that the ocean cooling contributed highly to Joaquin's intensification and decay.

THIS PAGE INTENTIONALLY LEFT BLANK

TABLE OF CONTENTS

THIS PAGE INTENTIONALLY LEFT BLANK

LIST OF FIGURES

LIST OF TABLES

THIS PAGE INTENTIONALLY LEFT BLANK

LIST OF ACRONYMS AND ABBREVIATIONS

ABI	Advanced Baseline Imager
ADT	Advanced Dvorak Technique
AMSU	Advanced Microwave Sounding Unit
AMV	Atmospheric Motion Vector
ATMS	Advanced Technology Microwave Sounder
CDO	central dense overcast
CIMSS	Cooperative Institute for Meteorological Satellite Studies
CIRA	Cooperative Institute for Research in the Atmosphere
COAMPS-TC	Coupled Ocean/Atmosphere Mesoscale Prediction System-Tropical Cyclone
ECMWF	European Center for Medium-range Weather Forecasts
FCDI	four-dimensional COAMPS-TC dynamic initialization
FNMOC	Fleet Numerical Meteorology and Oceanography Center
GFS	Global Forecast System
GOES	Geostationary Operational Environmental Satellite
IR	infrared
MSLP	minimum sea-level pressure
NASA	National Aeronautics and Space Administration
NAVGEM	Navy Global Environmental Model
NHC	National Hurricane Center
NOAA	National Oceanic and Atmospheric Administration
NOGAPS	Navy Operational Global Atmospheric Prediction System
NWP	Numerical Weather Prediction
OHC	ocean heat content
RI	rapid intensification
SATCON	satellite consensus
SCDI	SAMURAI COAMPS-TC dynamic initialization
SHIPS	Statistical Hurricane Intensity Prediction Scheme
SSEC	Space Science and Engineering Center
SSMIS	Special Sensor Microwave Imager/Sounder

SST	sea surface temperature
TC	tropical cyclone
TCI	tropical cyclone intensity
VWS-C	CIMSS vertical wind shear
VWS-S	SHIPS vertical wind shear

ACKNOWLEDGMENTS

I would like to thank Emeritus Professor Russell Elsberry and Professor Wendell Nuss for their advisory and mentorship roles in this thesis, as well as their comments on the manuscript. Many thanks to Mary Jordan, who helped with the data analysis for the horizontal plots of CIMSS VWS. Thank you to Chris Velden and Derrick Herndon of the Cooperative Institute for Meteorological Satellite Studies for providing the 15-min vertical wind shear calculations and the 30-min SATCON intensities. I am indebted to the Office of Naval Research (ONR) Tropical Cyclone Intensity (2015) field experiment for providing the datasets used throughout.

THIS PAGE INTENTIONALLY LEFT BLANK

I. INTRODUCTION

Tropical storms bring strong winds, high seas, heavy convection, and precipitation, all of which are detrimental to naval assets. With the logistics involved in keeping ships out of harm's way, it is imperative to have accurate forecasts for track and intensity of tropical storms as they possibly approach naval assets. This thesis will focus on Hurricane Joaquin (2015), which is one specific storm that caused particular issues for the Atlantic fleet concentration areas.

Hurricane Joaquin formed from a disturbance that had originated in the eastern North Atlantic and tracked northwestward of the Caribbean (Berg 2016). On 28 September 2015, the disturbance developed into a tropical cyclone (Figure 1). At the time of development, a blocking high was located over the western Atlantic that forced the storm to slowly track south-southwestward. As Joaquin moved over warmer waters near the Bahamas on 29 September, a period of rapid intensification (greater than 30 knots in 24 h) that lasted for 60 h was followed by the move over the Bahamas (Berg 2016). Joaquin then tracked over the Bahamas, which is when the ship SS *El Faro* sank, killing 33 people onboard. The *El Faro* accident may have been caused in part by changing and low-confidence forecasts (National Transportation Board 2017).

On 1 October, Hurricane Joaquin interacted with an upper-level trough that moved off the eastern United States, which caused Joaquin to reverse direction to the northeast from the Bahamas (Berg 2016). On 3 October, the blocking high had dissipated, which allowed Joaquin to accelerate northeastward while undergoing another intensification period. On 4 October, a deep low over the southeastern United States forced Joaquin to move more eastward until 6–7 October, at which time it interacted with the midlatitude flow, and the flow's vertical wind shear led to the dissipation of Joaquin as a tropical cyclone. During much of the life cycle of Joaquin, the Office of Naval Research-sponsored Tropical Cyclone Intensity (TCI) field experiment (Doyle et al. 2017) was collecting special datasets that will be utilized in this thesis.

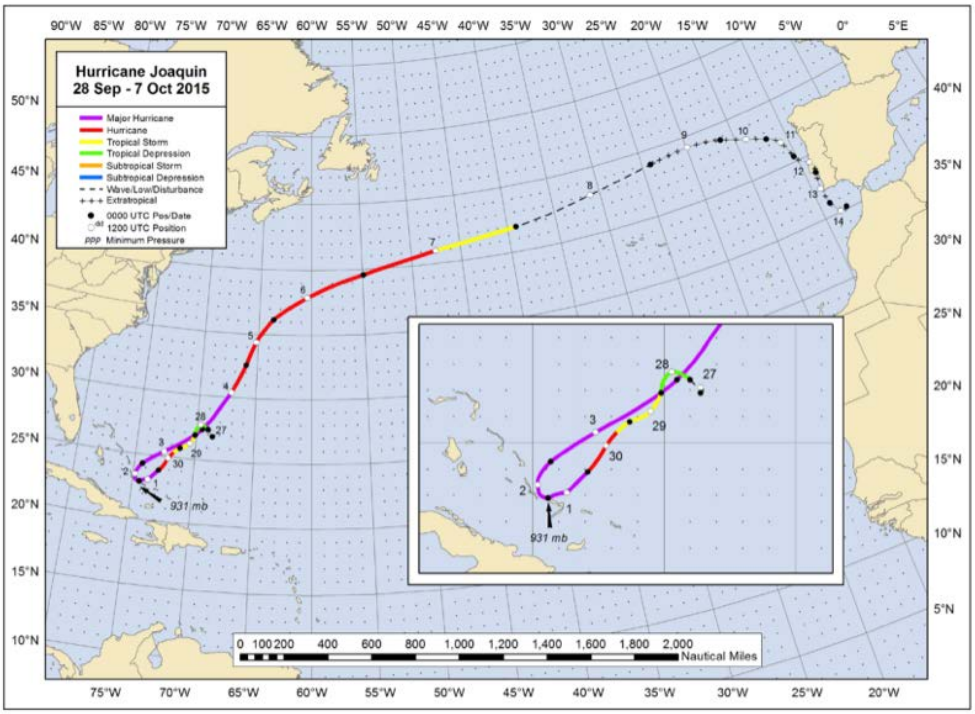

Best track positions for Hurricane Joaquin (2015) for the life cycle of the storm from 28 September 2015 to 7 October 2015.

Figure 1. Best-track positions for Hurricane Joaquin (2015). Source: Berg (2016).

During the period while Joaquin was moving southwestward toward the Bahamas, the track that Joaquin would subsequently have after leaving the Bahamas was poorly forecast by all U.S.-based models and by the National Hurricane Center (OFCL, Figure 2a). Usually reliable U.S. models such as Global Forecast System (GFSI, Figure 2b), Hurricane Weather and Research Forecast (HWFI, Figure 2d), Geophysical Fluid Dynamics Laboratory Experimental Model (GFEX, Figure 2e), and even the consensus of a number of these models (TVCA, Figure 2f) all forecast that after leaving the Bahamas, Joaquin would move toward the east coast of the United States. The only model that successfully forecast the sharp turn toward the northeast and track toward Europe was the European Center Medium-range Weather Forecast (ECMWF; Figure 2c). In Figure 2, the different tracks depicted are the forecast for each model between 0000 UTC 28 September to 1800 UTC 1 October. Therefore, the tracks for each model that are close to the best-

track (white track) are model runs later in Joaquin's life cycle after the track reversal began on 1 October.

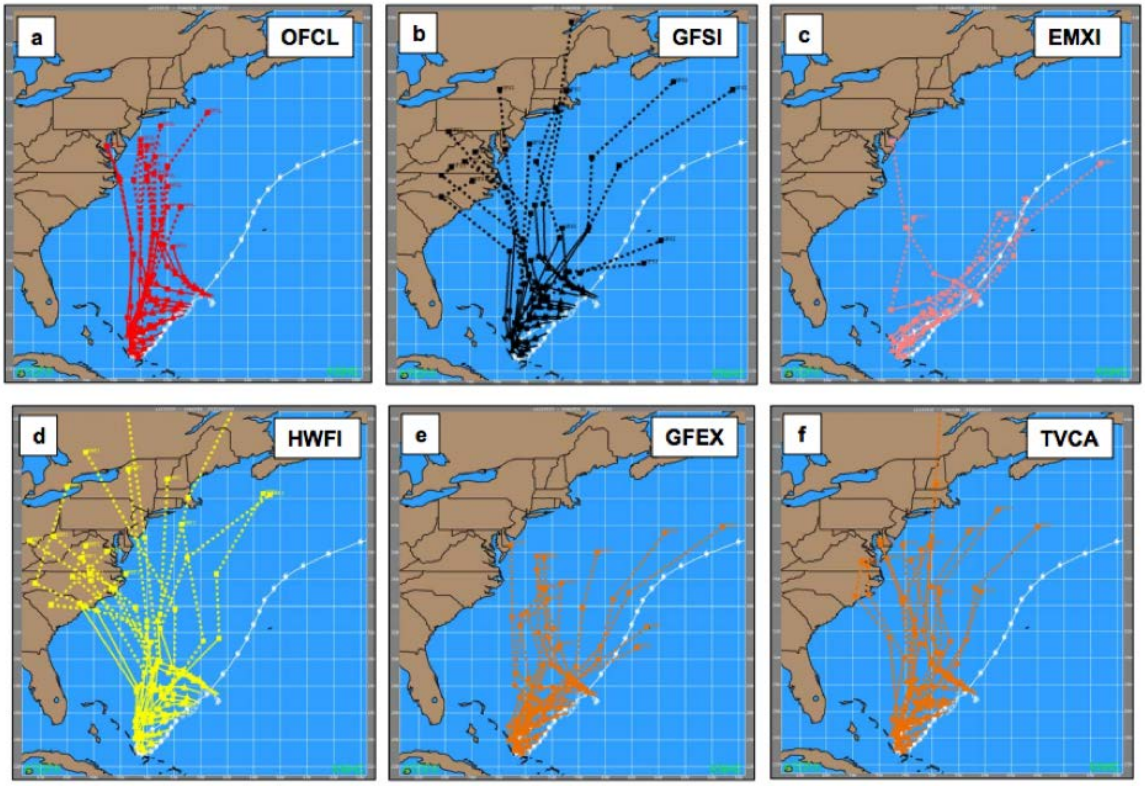

Comparison of Hurricane Joaquin best track (white symbols) with OFCL forecast from NHC (a) to GFSI (b), EMXI (c), HWFI (d), GFEX (e), and TVCA (f). [see text for model definitions]

Figure 2. Comparison of track forecasts with Hurricane Joaquin best-track. Source: Berg (2016).

The U.S.-based forecasts incorrectly had Joaquin moving directly toward the naval base in Norfolk, VA, when in reality the storm turned out to sea. However, the Navy utilized important assets to sortie ships from the Atlantic coast, which turned out to be unnecessary when Joaquin turned east to the Atlantic. With more accurate track forecasts that were consistent in time, the Navy would not have had to utilize those assets. One objective of this thesis is to demonstrate that using special observations such as the Tropical Cyclone Intensity (TCI) datasets in this thesis has the potential to substantially improve the Navy's ability to protect assets and make correct, informed decisions for the fleet assets. It

is imperative to continue development of these capabilities to allow warfare commanders to make better informed decisions to avoid damage or loss of life due to tropical cyclone activity without unnecessarily using assets to sortie the ships. In order to improve the forecast for Joaquin, it is necessary to answer the question as to whether the model forecasts were inaccurate because of the vortex structure or because of the environment modeled around the vortex. This thesis will provide evidence that it was at least partly due to the initialization of the environment that contributed to inaccurate forecasts of Joaquin.

Another objective of this thesis is to better understand the internal processes and environmental factors that contributed to the unusual southwestward track toward the Bahamas and the track reversal north of the Bahamas. In particular, one focus will be on the vertical extent of the inner vortex convection and the outflow level and strength. The hypothesis of this study is the addition of high temporal and spatial resolution Atmospheric Motion Vectors (AMVs) over the Joaquin vortex and in the surrounding environment will improve the vertical vortex structure and the outflow magnitude and structure that interacted with the adjacent upper-tropospheric troughs and ridge to cause the extreme track reversal.

In this thesis, Chapter II describes the datasets used and the method for analyzing the AMV datasets. The compilation of environmental factors affecting Joaquin is presented in Chapter III. The summary, conclusions, and future work are found in Chapter IV.

II. METHODOLOGY

A. DATASETS

The main dataset that will be used in this thesis is the Cooperative Institute for Meteorological Satellite Studies (CIMSS) special re-processed Atmospheric Motion Vectors (AMVs) in 15-min intervals from GOES-East that were produced for the entire life cycle of Hurricane Joaquin (2015) in support of the Office of Naval Research Tropical Cyclone Intensity (TCI-15) field experiment. This GOES-East dataset is intended to simulate the capability of the new generation GOES-16 satellite that has an Advanced Baseline Imager (Griffith 2015). This ABI has the capability to scan the full disk every 10–15 min in 16 different spectral bands. Three of these bands are in the visible spectrum and two are in the near-infrared spectrum. The visible bands range in spatial resolution from 0.5 km to 1.0 km, and the near-infrared bands have a spatial resolution of 2 km. This new ABI instrument is ideal for AMVs due to the improved ability to track clouds and water vapor features, which can be used to estimate winds throughout the troposphere (Velden et al. 2005). According to Elsberry et al. (2018),

> clouds or water vapor features can be selected from an image at time t and then the backward and forward motion vectors from t - 10 min to time t and from t to t + 10 min can be averaged to calculate AMVs at time t (rather than +/- 30 min as in the past). The individual AMVs are assigned heights (pressure levels) near the cloud-top or for water vapor features using multi-spectral techniques with accuracies of ± 25 hPa. Some limitations of present-day AMVs are that 30-min sampling frequency for tracking clouds is not optimal (Velden et al. 2005), and more rapid scanning sequences (1 to 5-min images) have been limited to restricted domains and durations. More importantly, applications in numerical weather prediction (NWP) have often been constrained to 6 h data assimilation cycles and AMV dataset thinning.

In this thesis, it will be demonstrated that shorter sampling times and continuous rapid-scanning combined with the advanced sensors on these new-generation satellites will substantially improve the quality and quantity of the AMVs, and thus their potential impacts on the Navy regional and global model analyses and predictions.

An example of these 15-min AMV fields around Hurricane Joaquin at 0015 UTC 30 September taken from the Office of Naval Research AMV dataset is shown in Figure 3. It will be demonstrated in Chapter III that these AMV wind vectors have the potential to add value to NAVGEM if they can be assimilated at high temporal resolution.

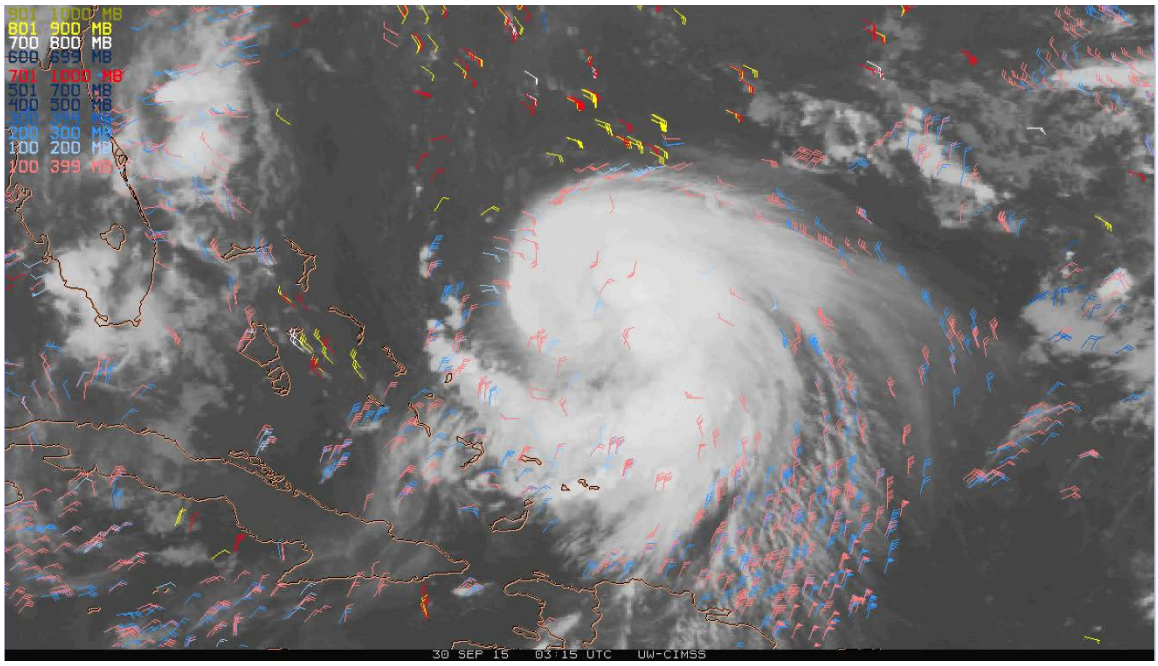

Example of AMV wind vectors at various levels (see color scale in upper left corner) around Hurricane Joaquin at 0315 UTC 30 September 2015.

Figure 3. Example of AMV wind vectors.
Source: Office of Naval Research (2015).

As described in Hendricks et al. (2018), a special CIMSS vertical wind shear (VWS) dataset was also created based on the 15-min AMVs. Hendricks et al. (2018) emphasized that the CIMSS VWSs are highly dependent on the AMVs rather than the background field of the Global Forecast System model. The special CIMSS VWS dataset based on the 15-min AMVs has the "TC vortex removed to a radius of 600 km in the 150–300 mb layer and to 800 km in the 700–950 mb layer wind analyses" (Hendricks et al. 2018). In this thesis, the CIMSS VWS vectors have been averaged over a circle of 350 km radius rather than the 500 km radius used by Hendricks et al. (2018) and Jorgenson (2017). This smaller averaging radius is selected because of the upper-tropospheric vortex of

Joaquin is confined by troughs to the west and to the east. It will be demonstrated in Chapter III that there are notable differences in timing of large intensity events throughout Joaquin's life cycle using the 15-min CIMSS VWS dataset.

According to Velden and Sears (2014), the CIMSS VWS is calculated after AMVs are assigned to gridded u and v wind fields. The VWSs are the vector differences between two layers at each grid point (700-925 hPa and 150-300 hPa), which then represent the environmental vertical wind shear above and below the cirrus canopy of the vortex. The vortex has been removed within a radius of 800 km in the lower atmospheric layer, and within 600 km in the upper atmospheric layer, in order to isolate the environmental shear. This thesis will examine area-averages of these VWS magnitude and direction, and also horizontal plots of the VWS vectors relative to the center of Joaquin.

Another dataset used for the analysis of the Joaquin evolution was a satellite consensus (SATCON) intensity dataset from the Space Science and Engineering Center (SSEC) at the University of Wisconsin-Madison. According to the CIMSS public information on this SATCON dataset (tropic.ssec.wisc.edu/misc/satcon/info.html), four satellite intensity algorithms are combined with a "statistically-derived weighting scheme" to increase the accuracy of the SATCON by emphasizing strengths and minimizing weaknesses of the individual intensity algorithms. As shown in Figure 4, the four algorithms used in the consensus are the CIMSS Advanced Technology Microwave Sounder (ATMS), the Cooperative Institute for Research in the Atmosphere (CIRA) ATMS, the CIMSS Advanced Microwave Sounding Unit (AMSU), and the CIMSS Special Sensor Microwave Imager/Sounder (SSMIS). The Advanced Dvorak Technique (ADT) algorithm comes from infrared imagers on geostationary meteorological satellites and is thus highly dependent on how clear the cloud structures etc., are in the storm at a particular time. The algorithms taken from microwave soundings are most accurate when the eye size of the storm is large compared to the field of view resolution of the instrument. Thus, the AMSUs and SSMIS are weighted heavier during times when the eye is larger in the storm. Temporal availability is also something considered when compiling the SATCON intensities. The ADT algorithms are highly accessible (at least 30 min on older

geostationary satellites). Since the microwave observations on polar orbiters are more sparse, those intensity estimates are interpolated to the hourly timeframes.

The SATCON intensities (red line, Figure 4) have noticeable deviations from the best track (black line) during the entire life cycle of Joaquin. These 30-min SATCON intensity values for Joaquin will be used in Chapter III as an alternative to the NHC best-track intensities because the SATCON values include details of Joaquin's intensification and decay that are smoothed over in the 6 h NHC best-track intensities that have traditionally been used for analysis.

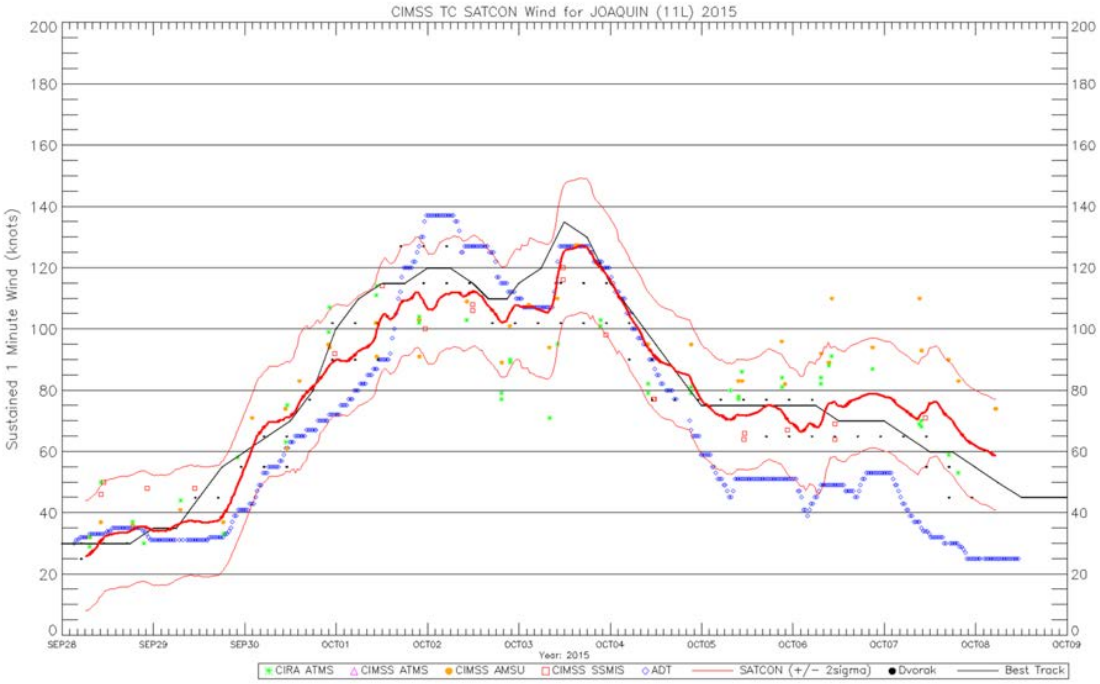

CIMSS tropical cyclone SATCON intensity values for Hurricane Joaquin including CIRA ATMS (green stars), CIMSS ATMS (magenta triangle), CIMSS AMSU (orange circles), CIMSS SSMS (red squares), ADT (black diamonds), SATCON intensity (red line), Dvorak values (black dots), and best-track intensities (black line).

Figure 4. CIMSS tropical cyclone SATCON intensity values.
Source: C. Velden, CIMSS (2018).

B. MODELS

The main model referenced in this thesis is NAVGEM, which is the Navy's global model run at Fleet Numerical Meteorology and Oceanography Center (FNMOC). Since there are both a deterministic and ensemble version of NAVGEM, the term NAVGEM in this thesis will refer to the deterministic model. The model is updated at 0600 UTC, 1200 UTC, 1800 UTC, and 0000 UTC daily, and the current version (NAVGEM 1.4) has an equivalent horizontal grid spacing of ~35 km. It has a Semi-Lagrangian/Semi-Implicit (SL/SI) dynamic core that allows for higher resolution than its predecessor (NOGAPS). It uses a Gaussian grid out to 180 h at 3 h intervals to complete each forecast cycle (Hogan et al. 2015).

In order to understand whether the model outputs are improved, it is important to understand how the atmosphere dynamics may have led to the Joaquin 180-degree track reversal. According to Berg (2016), a blocking ridge was present off the east coast of the United States just prior to the track reversal on 1 October 2015. In the comparison of the GFS and ECMWF forecasts at this valid time (Figure 5), it is evident that the GFS forecast had a weaker vortex for Joaquin, and also had a weaker ridge off the United States, than did the ECMWF forecast. Since ECMWF was the only model that predicted this segment of Joaquin's track correctly, and the stronger ridge and deeper vortex in the ECMWF model may be attributed to the atmospheric initialization. Of note, model physics could also be a contributing factor for a 72 h forecast (Figure 5). The atmospheric initial conditions for NAVGEM will be examined as the likely explanation for why NAVGEM failed to predict the post-reversal track of Joaquin.

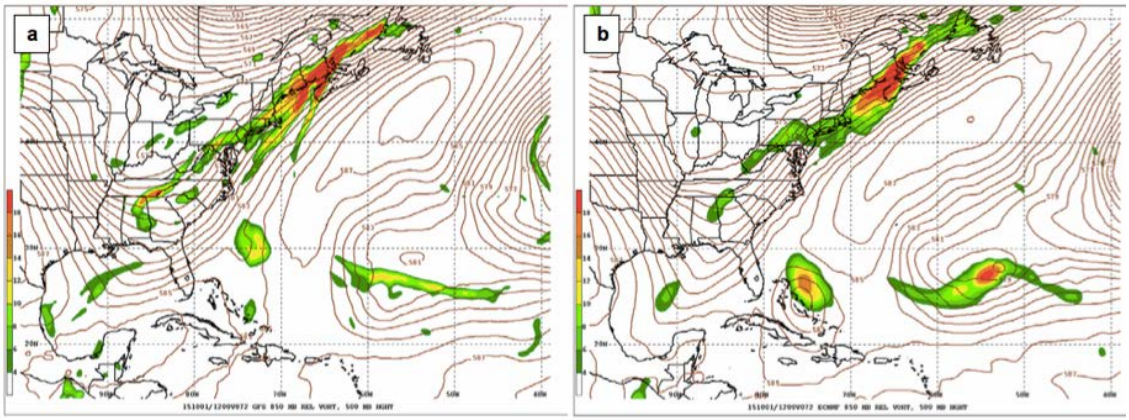

Model 72-h forecast fields for 850 mb relative vorticity (shading) and 500-mb heights at 1200 UTC 1 October 2015 from (a) GFS and (b) ECMWF models.

Figure 5. Model 72-h forecast fields (850 mb relative vorticity and 500 mb heights). Source: Berg (2016).

In the current version of NAVGEM, the initialization involves both a "cold start" and a synthetic vortex. When a new storm is predicted by NAVGEM, no atmospheric dynamics before the first model run are taken into account, so it takes multiple model runs for the storm to be accurately modeled. The synthetic vortex in NAVGEM is an idealized vortex that only extends to 400 mb, which means the outflow layer of the storm is not included. Thus, adding accurate AMV observations to represent the steering winds inside the synthetic vortex and the wind structure in the outflow layer and in the surrounding environment could substantially improve the track and intensity forecast.

Berg (2016) summarized the Minimum Sea Level Pressure (MSLP) and V_{max} for 30 h before and after the time in Figure 5 (Table 1). Note that the MSLP rapidly decreases and V_{max} rapidly increases through this period until 0000 UTC 2 October. Clearly, the GFS forecast in Figure 5a does not have such an intense vortex, and the GFS short-wave trough position near 30 N, 75 W is not consistent with the 1200 UTC 1 October position (23.1 N, 73.7 W) in Table 1. Indeed, the Joaquin circulation in the GFS forecast is moving poleward in response to the 500 mb trough to the west (not shown). By contrast, the ECMWF forecast has a more intense circulation near 24 N, 76 W, which is much closer to the actual position in Table 1. Thus, properly modeling the southwestward track to the Bahamas as in Figure 5 and Table 1 may be critical to a correct forecast of the track reversal of Joaquin.

Table 1. Hurricane Joaquin Best-track position and intensity information. Source: Berg (2016).

Date/Time	Latitude(degN)	Longitude(degW)	Pressure (mb)	WindSpeed (kt)
30/0600	25.4	71.8	978	65
30/1200	24.9	72.2	971	70
30/1800	24.4	72.5	961	80
01/0000	23.9	72.9	951	100
01/0600	23.5	73.3	947	110
01/1200	23.1	73.7	942	115
01/1800	23.0	74.2	936	115
02/0000	22.9	74.4	931	120
02/0600	23.0	74.7	935	120
02/1200	23.4	74.8	937	115
02/1800	23.8	74.7	941	110

Location, pressure (MSLP) and maximum wind speeds of Hurricane Joaquin from 0600 UTC 30 September 2015 to 1800 UTC 2 October 2015.

THIS PAGE INTENTIONALLY LEFT BLANK

III. OBSERVATIONS OF ENVIRONMENTAL FACTORS AFFECTING JOAQUIN

This thesis is an extension of previous studies at the Naval Postgraduate School that have focused on environmental VWS and its impacts on TC intensity evolution. Jorgenson (2017) showed the environmental VWS variations could better explain (relative to other environmental factors) Joaquin's rapid decay, the interruption of the rapid decay, and the subsequent constant intensity as the storm translated northeastward over colder waters in the Atlantic. Hendricks et al. (2018) then further validated strong VWSs did contribute to the rapid decay of Joaquin, and that the VWS concentrated in the upper troposphere modified the vertical structure of the warm core vortex to impact intensity changes through the latter half of the Joaquin life cycle. The methodology and interpretations of environmental VWS impacts in these previous research studies was a motivation to continue the examination of these environmental factors on Joaquin using high temporal and spatial resolution AMV datasets in this chapter. Specifically, this thesis will examine how the VWS may have affected the rapid intensification events as well as the track reversal of Joaquin.

A. JOAQUIN INTENSITY CHANGE IN RELATION TO SHIPS VWS

The typical strategy for such an environmental analysis is to linearly correlate 6 h values of VWS with 6 h changes of intensity, usually with intensities from the NHC best-track file published after the storm season. The diagnosis of the environmental factors affecting the intensity changes during the southwestward track to the Bahamas and during the northeastward track away from the Bahamas follows the methodology of the Jorgenson (2017) and Hendricks et al. (2018) studies. Jorgenson (2017) showed

> that among the Hendricks et al. (2010) environmental factors that best compared with the Joaquin intensity changes was the VWS from either the SHIPS or the CIMSS technique (Gallian and Velden 2002; Velden and Sears 2014). Whereas the SHIPS VWS (hereafter VWS-S) is simply the difference between the GFS 200 and 850 hPa horizontal wind analyses, the CIMSS VWS (hereafter VWS-C) utilizes a local three-dimensional analysis

> of high-density, satellite-derived AMVs to calculate horizontal wind analyses at mandatory levels with much less dependence on the 6-h GFS forecast as a background than does the SHIPS technique. Then the VWS-C is the vector difference between the pressure-weighted mean wind fields in the 150–300 hPa and the 700–950 hPa layers. Both approaches use a vortex-filtering methodology in the final VWS estimate.

Some limitations of only having these VWS products at 6-h intervals are illustrated in Figure 6. Note especially the large VWS-S changes at 0300 UTC 4 October and 2100 UTC 4 October, but also note the smaller deviations at 1500 UTC 29 September and 2100 UTC 5 October from smoother time variations that might be expected for large-scale environmental VWS. Hendricks et al. (2018) suggested several reasons for the large 6-h VWS-S variability in Figure 6 from 0300 UTC 4 October and again from 2100 UTC 4 October to 0300 UTC 6 October. The VWS-S during 2015, according to Hendricks et al. (2018),

> was being calculated based on background 6-h GFS forecasts that included hourly AMVs (thus utilizing ± 30-min images), but only at the 6-h synoptic times, which may explain the 6-h variability. Furthermore, the AMVs incorporated in the data assimilation for the GFS had been thinned to be appropriate for the effective GFS horizonal grid resolution. Finally, the quality control criteria between the AMV magnitudes and directions were being applied relative to the wind fields in a model-predicted TC vortex that had been relocated from the 6-h GFS forecast position to the observed position. If those AMVs indeed reflect the real Joaquin vortex structure and outflow, the AMVs may easily have been rejected in the quality control step because of their substantial deviations from the GFS vortex structure and outflow.

The linear correlation coefficient of the 6 h VWS-S with the NHC best-track intensities every 6 h in Figure 6 is only 0.0131, which of course is an insignificant correlation. Part of this lack of correlation may be because the NHC best-track intensities are only digitized in 5 kt increments, which leads to two periods of constant intensity changes of -10 kt per 6 h between 0300 UTC 4 October and 2100 UTC 4 October and 0 kt per 6 h between 0300 UTC 5 October and 0300 UTC 6 October when the VWS-S were rapidly varying in magnitude.

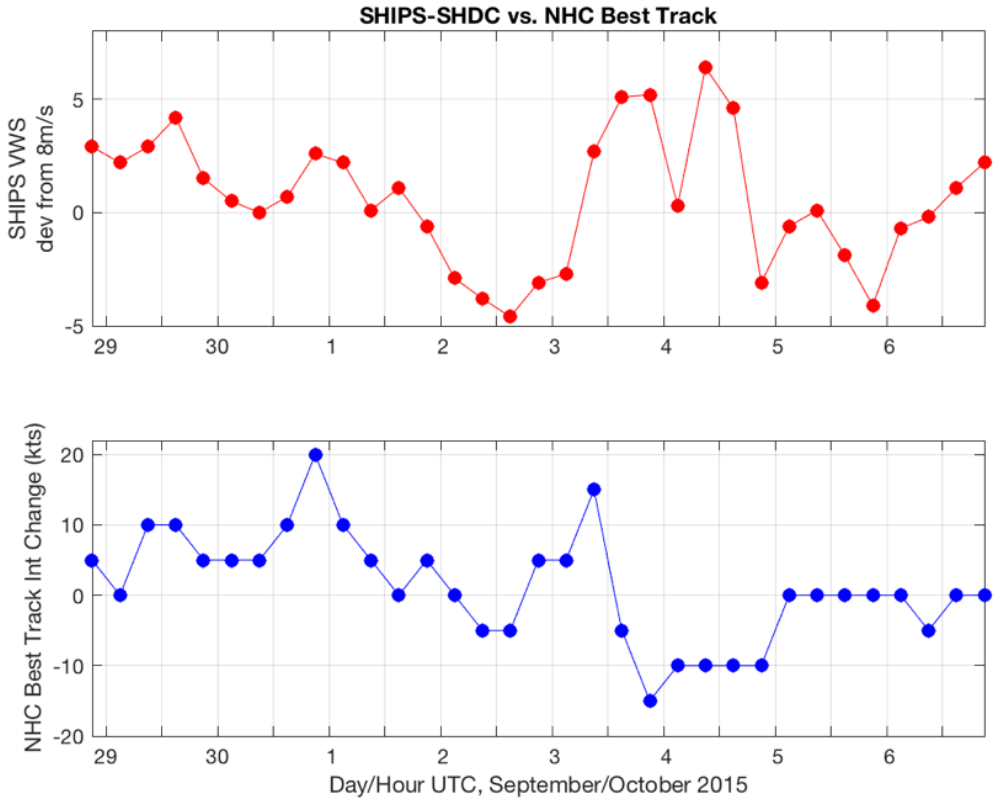

SHIPS Vertical Wind Shear (VWS) deviation from 8 m/s (moderate wind shear) (top) and the NHC best-track intensity change (bottom) every 6 h.

Figure 6. SHIPS VWS deviations and NHC best-track intensity change

Elsberry et al. (2018) questioned the NHC best-track intensity (V_{max}) changes during the interrupted rapid decay followed by a constant intensity of 75 knots for 30 h, because both the Navy regional model (COAMPS-TC) and the NAVGEM failed to predict the abrupt ending of the rapid decay of Joaquin at 0000 UTC 5 October. Rather than predicting a 30-h period of constant intensity of 75 knots, these Navy models predicted a continued (but slower) decay for approximately 12 h and then a re-intensification to 75 knots. However, the Minimum Sea Level Pressure (MSLP) increase for 12 h following 0000 UTC 5 October and then a near-constant MSLP as in the NHC best-track files was well predicted by the COAMPS-TC. Co-author Chris Velden (personal communication, May 2017) of Elsberry et al. (2018) had simply noted that satellite-based intensity (V_{max})

estimates could be found that also continue the rapid decay beyond 0000 UTC 5 October with a subsequent re-intensification.

These questions about the NHC best-track intensities following 0000 UTC 5 October was part of the motivation in this thesis to also examine the SATCON intensity (V_{max}) changes for Joaquin as shown in Figure 4 as an alternative to the NHC best-track intensities. Hendricks et al. (2018; in their Figure 2) had also compared the 6 h VWS-C that primarily depend on carefully quality controlled AMVs with the 6 h SHIPS-SHDC VWSs from 0000 UTC 3 October through 0000 UTC 6 October and found that these 6 h VWS-C were much more smoothly varying than the VWS-S in Figure 6. This VWS comparison was the motivation for Hendricks et al. to create a VWS-C dataset at 15-min intervals from the AMVs at 15-min intervals. Examples of the horizontal distributions of these 15-min VWS-C vectors relative to the position of Joaquin at four times corresponding to the NASA WB-57 aircraft missions were provided in Figure 2 of Hendricks et al. (2018). In this thesis, these 15-min VWS-C will also be averaged over a circle of 350 km radius centered on the Joaquin position. The reduction from an averaging radius of 500 km utilized in Hendricks et al. (2018) was based on the horizontal scales of these VWS-C vectors based on the 15-min AMVs (see Chapter III Section C).

B. JOAQUIN INTENSITY CHANGE IN RELATION TO VWS-C

The raw 6-h changes in the 30-min SATCON intensities and the 15-min VWS-C magnitude and direction evolutions are shown in Figure 7. Because the 30-min SATCON intensities in Figure 4 have short-term variability, the 6-h intensity changes have even larger variability such that the synoptic timescale trends are obscured (Figure 7, top). For correlation analysis comparable to the VWS-S versus NHC intensity correlation, the 30-min SATCON intensities in Figure 4 are first averaged over a 6-h period (i.e., ± 3 h) to provide values at traditional synoptic times (0000 UTC, 0600 UTC, 1200 UTC, and 1800 UTC). The 15-min VWS-C directions (Figure 7, middle) and the magnitudes, which are expressed as deviations from a "moderate" value chosen to be 8 m s^{-1} (Figure 7, bottom) are averaged for the 6 h between these synoptic times and thus apply at the mid-point of the 6 h SATCON intensity changes (Figure 9). For example, the 15-min VWS-C

magnitudes in Figure 7 (bottom) from 0000 UTC to 0600 UTC are averaged and assigned to 0300 UTC, and the correlation will be with SATCON intensity change (0600 UTC minus 0000 UTC) that is also at the midpoint time (see Figure 9). During the period between 0000 UTC 30 September and 1200 UTC 2 October, the VWS-C directions rotate between west of north and east of north, so special averaging was required. Although the correlations will first be over the entire period, a special focus will be on the early part of Joaquin, and on the rapid intensification events. Note in Figure 6 that the NHC best-track file has the first rapid intensification peaking between 1800 UTC 30 September and 0000 UTC 1 October, which is a full day later than in the SATCON dataset (Figure 9), which has the first rapid intensification event peaking between 1800 UTC 29 September and 0600 UTC 30 September.

Another useful comparison between datasets is the track based on the SATCON data and the NHC best-track data (Figure 8). These SATCON position values are averaged over a 6 h period around a midpoint of 0000 UTC, 0600 UTC, 1200 UTC, or 1800 UTC and then the average value is assigned to the corresponding synoptic time. By averaging the SATCON positions in this manner, the track positions could be directly compared to the 6 h NHC best-track positions. The most notable difference during the Joaquin track reversal is that the SATCON track is farther west than the NHC best-track from 1200 UTC 30 September until about 3 October. Possible reasons for this difference will be discussed later in this chapter. It is also notable that the SATCON track starting on 4 October veers far east of the NHC best-track, and thus the 0600 UTC 4 October position near 28.8 N, 67.8 W is about 0.1 deg. lat. south and more than a 0.6 deg. long. east of the NHC best-track position.

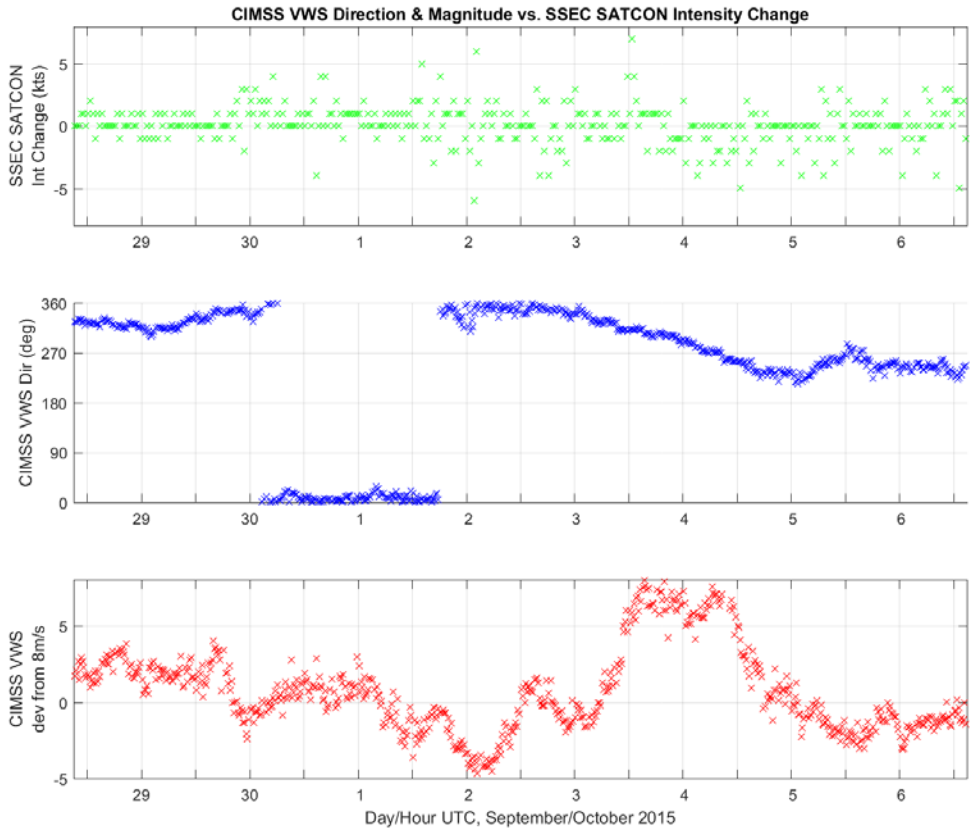

SSEC 30-min SATCON intensity change (top), VWS-C direction (middle), and CIMSS 15-min VWS magnitude deviations from moderate shear (8 m s^{-1}) (bottom).

Figure 7. CIMSS VWS deviations, VWS direction, and SATCON intensity changes

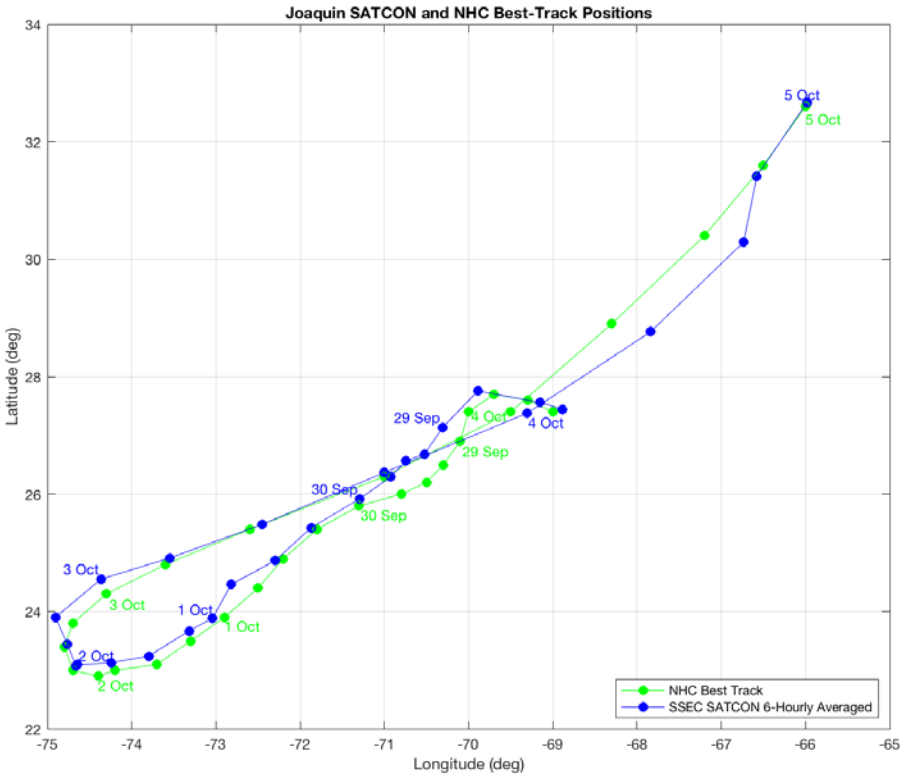

The NHC best-track 6-h positions (green) are from Berg (2016). The SATCON 6-h positions (blue) are derived from the ADT positions and are averaged over the same 6 h times as the VWS-C. Date/month positions at 0000 UTC of the SATCON and NHC best-track are indicated.

Figure 8. SATCON and NHC best-track positions of Joaquin 0000 UTC 28 September to 0000 UTC 5 October

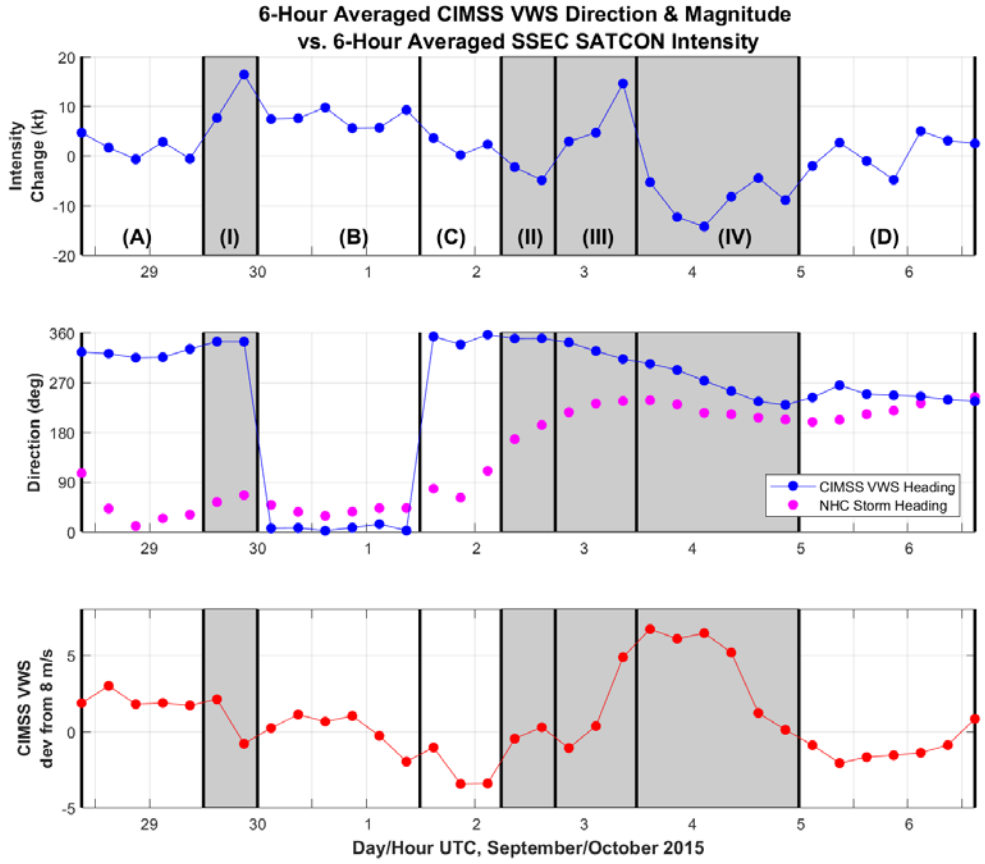

6-h averaged SSEC SATCON intensity changes for the storm (top), 6-h averaged VWS-C direction (blue dots) and storm heading (pink dots) (middle), and 6-h averaged VWS-C deviations from 8 m/s (bottom). Gray shaded areas are events discussed in Chapter III and lines delineate nonlinear intensity change segments discussed in Chapter III.

Figure 9. 6-h average CIMSS VWS deviations, VWS direction, storm heading, and SATCON intensity change.

The linear correlation coefficient of -0.36 between the 6-h average SATCON intensity changes and the deviations of the 6-h average 15-min VWS-C from a moderate VWS of 8 m s^{-1} in Figure 9 is much higher than the 0.01 correlation of the VWS-S with the NHC intensity changes in Figure 6. This result that the correlation was higher is promising and suggests that using a VWS dataset with a higher temporal and spatial resolution could yield a more accurate depiction of Joaquin's intensification and rapid decay. Even when the VWS-C were correlated with the NHC intensity changes (not shown), a higher correlation of - 0.25 was obtained. These larger correlation coefficients indicate that it is the improvement of the 15-min VWS-C relative to the VWS-S that is the major contribution to the correlation of VWS to intensity change. However, the utilization of the smoothed, high frequency SATCON intensities versus the 6-h NHC best-track intensity changes also has a substantial contribution. An examination of the reasons why the best-track intensities lead to a lower correlation with the VWS-C is outside the scope of this thesis.

One of the contributions to the higher correlation of the VWS-C with the SATCON intensity changes is that the first rapid intensification in the SATCON dataset with a maximum of about 19 kt in 6 h is coincident in time with a decrease in VWS at 2100 UTC 29 September. By contrast, the first rapid intensification in the NHC best-track file peaked at 2100 UTC 30 September when the VWS-S was about 11 m s^{-1} (Figure 6), and the VWS-C deviation from 8 m s^{-1} was more in the moderate range with a value of +1 m s^{-1}. It is noteworthy that the VWS-C direction (Figure 9, middle) rotated through north following the first RI to become more aligned with Joaquin's direction. Both the SATCON and the NHC best-track have the second rapid intensification event peaking at 0900 UTC 3 September at a time when both the VWS-C (Figure 9) and the VWS-S (Figure 6) are becoming large (+ 5 and + 3 m s^{-1} relative to a moderate VWS of 8 m s^{-1}, respectively). At this time, the contribution to the correlation coefficient would actually be positive.

Another counter-intuitive feature in Figure 9 is that from 0900 UTC 1 October to 0300 UTC 2 October the VWS-C are becoming smaller, but the SATCON intensity change magnitudes are also becoming smaller. Although the VWS-C then increase to moderate

values (~ 8 m s^{-1}) at 0900 UTC 2 October, the SATCON intensity change is actually a decay of 5 m s^{-1} per 6 h at 1500 UTC 2 October just before the start of the second rapid intensification event. These counter-intuitive intensity changes are occurring during the Joaquin track reversal from a heading of 030 deg (toward the south-southeast) at 0900 UTC 1 October to a heading of 240 deg (toward the east-northeast) at 0300 UTC 3 October (Figure 9, middle).

In summary, simply calculating a linear correlation coefficient over the entire storm life cycle may be obscuring important physical processes in the environmental interaction with Joaquin. Thus, the Joaquin intensity evolution will be separated into four events, and the VWS-C direction and the storm heading illustrated in Figure 9 (middle) will be considered in relation to these intensity change events. The ultimate objective is to understand how these environmental VWS and internal responses in terms of intensity changes may be related to the change in storm heading from toward the southwest to toward the northeast during the Joaquin track reversal.

C. NONLINEAR INTENSITY CHANGE SEGMENTS AND EVENTS IN RELATION TO ENVIRONMENTAL VWS

After assessing the results of the environmental analysis above, four events (shaded areas in Figure 9) and four distinct intensity change segments of the storm have been defined (Table 2). These events and segments were chosen by first selecting events of interest over the life cycle of Joaquin. Two RI events (Events I and III), a period of intensity decrease in low VWS (Event II), and the rapid decay after a RI (Event IV) were chosen as stages that needed further investigation. Segments were then chosen as phases to understand factors that may have contributed to the defined events or phases to study the impacts of the defined events on the environmental VWS and intensity change. Recall that the intensity changes are per 6 h, but the traditional definition of a rapid intensification (RI) of 30 kt/day will be applied in defining events (and for rapid decay). When discussing the VWS-C, the moderate VWS has been tentatively defined as being centered on 8 m s^{-1}, but it is uncertain how broad this moderate VWS range should be. Thus, high VWS will be defined as above 10 m s^{-1}, and low VWS is defined as below 6 m s^{-1}. The mean 6-h average

values of various parameters for each segment are summarized in Table 2 to give a concise overview of their variations between segments of the storm defined above.

Segment A from 0900 UTC 28 September to 0900 UTC 29 September precedes the time before the first rapid intensification (Event I), which according to the SATCON peaked between 1500 UTC 29 September to 2100 UTC 29 September. During the second segment (Segment B) of the storm from 0300 UTC 30 September to 0900 UTC 1 October after the first rapid intensification, the intensity changes were steadily between 3–5 kt per 6 h, which over 24 h would approach the traditional rapid intensification definition of 30 kt per day. As will be described below, this continued RI may be related to the rotation of the VWS-C direction to become east of north. The third segment (Segment C) is a period of the storm (1500 UTC 1 October to 0300 UTC 2 October) when the direction of VWS-C has rotated back to being west of north but is also of much interest because it is when the track reversal occurs (Figure 9). The next event of the storm is that counter-intuitive Event II mentioned above that is characterized by decreasing intensity in low VWS-C that occurs between 0900 UTC 2 October to 1500 UTC 2 October. Event III of the storm from 2100 UTC 2 October to 0900 UTC 3 October includes the second rapid intensification event that appears in Figure 9 to be almost concurrent with a rapid increase in VWS-C. The next Event IV of the storm from 1500 UTC 3 October to 2100 UTC 4 October includes the extremely rapid decay with a subsequent slight re-intensification as Joaquin moves poleward over cold water and transitions to an extratropical cyclone. This last event and Segment D during 0300 UTC 5 October to 1500 UTC 6 October are the interrupted rapid decay and subsequent constant intensity period as discussed in Elsberry et al. (2018) and Hendricks et al. (2018).

Table 2. Definition and characteristics of Joaquin intensity change segments and events

Segment	Intensity Change/6 h (kt)	VWS Magnitude dev from 8 m s^{-1}	VWS-C / SATCON correlation	VWS-C Heading (deg)	Storm Heading (deg)	Magnitude of Delta S.H & VWS (deg)
A: 28/09Z – 29/09Z	1.6	2.0	0.12	304	043	261
B: 30/03Z – 01/09Z	7.5	0.11	-0.34	006	039	033
C: 01/15Z – 02/03Z	0.96	-2.6	0.79	349	083	094
D: 05/03Z – 06/15Z	0.77	-1.1	0.19	252	221	031
Event:	**Intensity Change/6 h (kt)**	**VWS Magnitude dev from 8 m s^{-1}**	**VWS-C / SATCON correlation**	**VWS-C Heading (deg)**	**Storm Heading (deg)**	**Magnitude of Delta S.H & VWS (deg)**
I: 29/15Z – 29/21Z	12.0	0.64	-1.0	288	060	132
II: 02/09Z – 02/15Z	-3.6	-0.12	-1.0	265	180	085
III: 02/21Z – 03/09Z	7.4	1.36	1.0	313	228	085
IV: 03/15Z – 04/21Z	-8.9	4.27	-0.4	268	217	051

Average values of intensity change per 6 h (SATCON), vertical wind shear (VWS-C) magnitude deviation from moderate wind shear, correlation coefficient of VWS-C magnitude deviation from moderate VWS-C and intensity change, VWS-C direction, storm heading (NHC Best Track), and the difference between the storm heading (S.H.) and vertical wind shear heading. Dates/times are in zulu (Z=UTC)

The correlations in Table 2 were calculated at synoptic times after averaging the 15-min VWS-C and the 30-min SATCON values over 6 h. Whereas the correlations during the short Events I, II, and III are high (1.0 or -1.0) due to the short time averaging (sometimes based on only 24 points), the key point in this thesis is that the correlations during an event may be positive as well as negative. Thus, a linear correlation of VWS and intensity over the entire Joaquin lifecycle does not accurately depict the environmental impacts on the intensity changes. This is the motivation for designing segments and events to more accurately depict rapidly changing effects of the environmental VWS on intensity changes.

1. Segment A and Event I: Pre-rapid Intensification and First Rapid Intensification

Berg (2016) focused on some key events that led to the different phases of Joaquin's life cycle shown in Figure 9. Berg (2016) states that it was the north-northwest shear (based on VWS-S) that prevented Joaquin from strengthening during Segment A, and that the "blocking ridge of high pressure located over the western Atlantic" was the driving force that steered Joaquin in southwestward motion. Berg (2016) also notes that around 0000 UTC 29 September, Joaquin moved over very warm water (30 deg C), and that NHC declared Joaquin to be a Tropical Storm at 1200 UTC 29 September.

Based on the VWS-C at 15-min intervals that have been smoothed over 6-h intervals, during Segment A the VWS magnitude as a deviation from a moderate value of 8 m s^{-1} was + 2.0 m s^{-1} and had a heading of 304 deg (from the west-northwest) (Table 2, row 1). Thus, this strong VWS was impinging almost perpendicularly on pre-Joaquin that had a storm heading of 043 deg (from the northeast). Thus, it is not surprising that the average 6 h intensity change is only 1.6 kt during Segment A according to the SATCON estimates. Although the correlation coefficient is small (0.12), it is noteworthy that the sign is positive, i.e., pre-Joaquin is slightly increasing under larger than moderate VWS-C.

As discussed earlier, the first rapid intensification (RI) of Joaquin peaks at 2100 UTC 29 September according to the SATCON estimates (Figure 9), but not until 2100 UTC 30 September for the NHC best-track (Figure 6). This SATCON peak intensity

change at 2100 UTC 29 September correlates exactly in time with the decrease in VWS-C (Figure 9). While the VWS-C did decrease, it only decreased into the moderate range to a minimum of 8.64 m s^{-1} averaged over Event I (Table 2, row 5). Even with this small decrease over a short period, the average intensity change of 12 kt per 6 h led to a correlation coefficient of –1.0, which is the expected negative correlation with a decrease in VWS leading to an intensification. However, in this case it was only a small decrease into the moderate VWS that was associated with a RI.

Note also that this RI event occurs with small changes in the VWS-C heading, which is still almost 90 deg off of the storm heading (storm heading southwestward while the VWS-C heading is from the west). However, between 1215 UTC and 1515 UTC 29 September the VWS-C direction shifts to a more northerly direction (Figure 10). Synoptically, the VWS-C shift appears to be a part of the ridge off the southeast coast of the United States building farther into the Atlantic. Although the VWS-C is evolving, it is unclear how this slight VWS-C shift 3 h prior to the peak RI may have been contributing to the RI event. Of note, it is also likely that Joaquin's translation over warmer waters contributed to the RI as well.

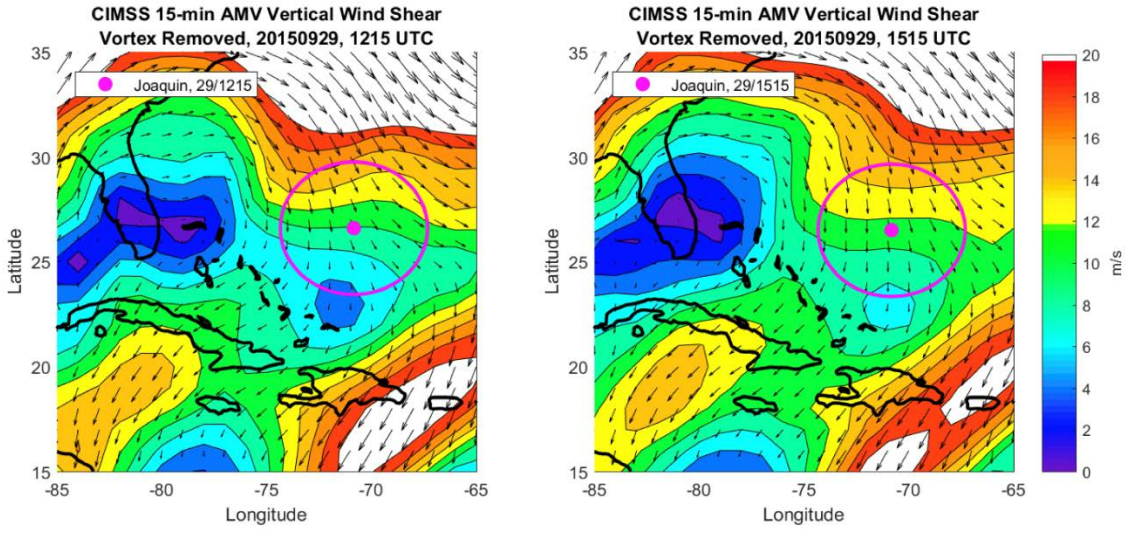

Horizontal plots of the VWS-C vectors relative to the SATCON position of Joaquin (magenta dot) during the first RI. The VWS-C values in Figure 9 and Table 2 are averaged over the circle with a radius of 350 km (left) 1215 UTC and (right) 1515 UTC 29 September. Source: Mary Jordan, NPS.

Figure 10. CIMSS VWS vector field for first RI event

A GOES-East infrared satellite image at 1815 UTC 29 September about three h prior to the SATCON first peak RI reveals a well-defined central dense overcast (CDO) with strong outflow from the north-northeast anticyclonically around to the south-southwest semi-circle (Figure 11). However, the outflow is constrained in the entire northwest quadrant of the CDO, which is consistent with VWS-C vectors to the northwest of the Joaquin center in Figure 10. Whereas those vectors appear to indicate that the VWS-C vectors have penetrated to the center, it is clear from this satellite image (Figure 11) that the strong outflow in the northwest quadrant has "fought-off" the impinging VWS. Elsberry and Jeffries (1996) had noted such an interaction between the outflow of Typhoon Robin (1993) had modulated the development of Tropical Storm Steve (1993). Elsberry and Park (2017) had suggested that such an outflow-VWS interaction was a contributing factor in the timing of the rapid intensification of Hurricane Earl (2010). Thus, an explosive deep convection burst must have occurred during the first RI event of Joaquin such that the outflow in the northwest quadrant was able to prevent the VWS associated with the flow from the northwest from penetrating to the center.

2. Segment B: Post-rapid Intensification and Shift in VWS-C Directions

The post-RI Segment B is an interesting period as Joaquin continued to intensify at an average rate of 7.5 kt per 6 h (Table 2, row 2), which then meets the 30 kt / 24 h criteria for a steady, extended (30 h) rapid intensification. Again, this extended RI occurred in a moderate VWS of 8.11 m s^{-1}, with a correlation coefficient of –0.34. While Joaquin was still moving southwestward (heading 039 deg), the VWS-C had a heading of 006 (from the north) (Table 2, column 4) so that VWS vector was nearly aligned with the storm heading. Consequently, the tilt of the vortex due to the following VWS-C may be contributing to the continued RI as the warm core aloft is being advected in the same direction as the low-level pressure center of Joaquin. Further study is needed to validate this hypothesis.

During segment B and continuing into segment C, Berg (2016) notes that the "mid- to upper-level trough over the eastern United States deepened on 1 and 2 October," which Berg (2016) attributes to be the cause of Joaquin's track reversal. As an alternative to this remote environmental cause, other contributions to the track reversal may be related to the

VWS-C heading changes during Segment B (Figure 7). At 0915 UTC 30 September (Figure 12, upper left), there are areas of VWS-C of equal strength to the east and west of the storm. However, the VWS-C to the west is heading southwest, while to the east of the storm the VWS heading is toward the south-southeast. When averaged over the 350 km area, the average VWS-C heading is 006 deg (Table 2, column 4). At 1515 UTC 30 September (Figure 12, upper right), the largest VWS-C values are to the east of the Joaquin center and heading south-southeast. By 0315 UTC 1 October (Figure 12, lower left), the gradient of south-southeast VWS-C has become stronger to the southeast of Joaquin. That VWS-C gradient relaxes again by 1215 UTC 1 October (Figure 12, lower right). Note that these changes in VWS-C direction and location relative to the Joaquin center occurred in less than a day.

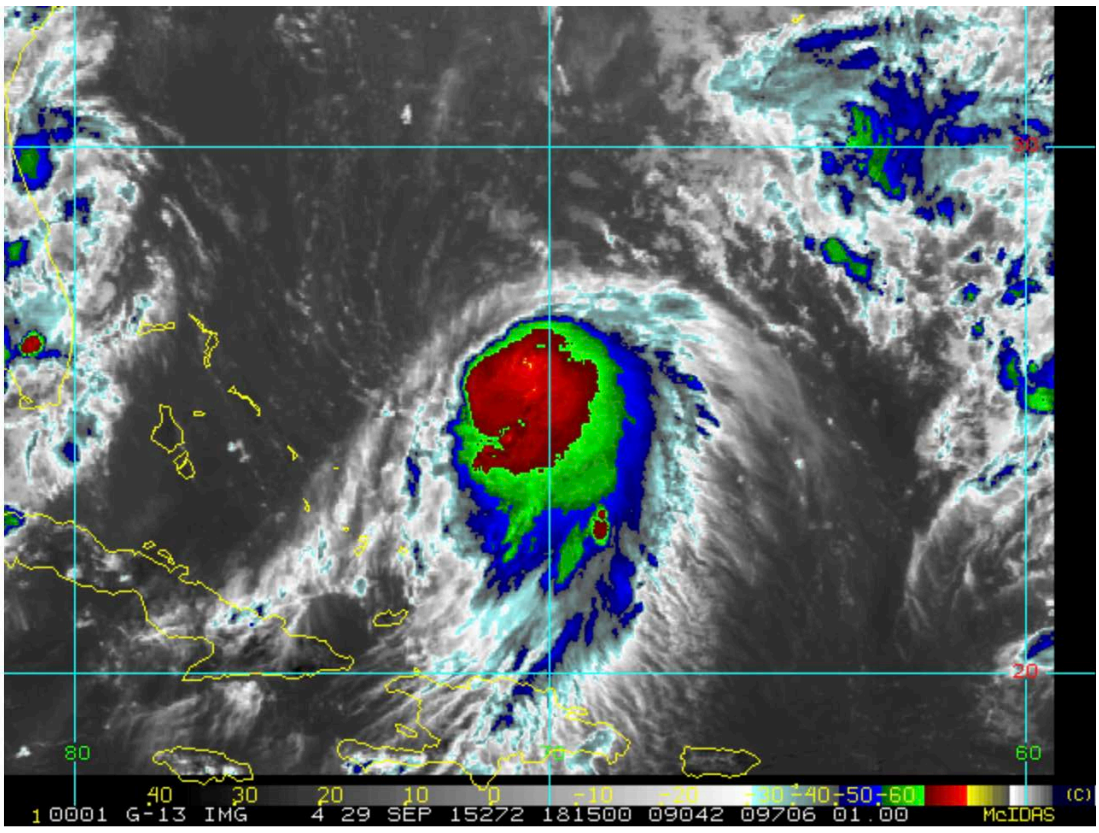

Remapped infrared imagery (~11 μm) at 4 km resolution taken from geostationary satellites (GOES-East) at 1815 UTC 29 September 2015.

Figure 11. Enhanced IR satellite picture of Joaquin 1815 UTC 29 September. Source: NOAA Satellites and Information, Regional and Mesoscale Meteorology Branch (RAMMB) (Accessed: 21 February 2019).

The horizontal plots of the VWS-C vectors suggest as well that the large area of smaller VWS-C magnitudes shifted from southwest of Joaquin (Figure 12, upper left) to northwest (Figure 12, upper right), and then directly north of Joaquin (Figure 12, lower left and lower right). These position shifts of Joaquin relative to the near-zero VWS-C region may certainly have contributed to the continued RI during segment B (Figure 9). Furthermore, these Joaquin position shifts may also have contributed to the track reversal that occurred less than a day later. That is, the anticyclonically turning of the enhanced outflow appears to have “pushed to the east” the north-south band of large VWS-C in Figure 12 (lower right) such that the 8 m s^{-1} moderate VWS isoline of VWS-C at 23 deg N is to the east of the center near 72 deg W. By contrast, 21 h earlier (Figure12, upper right), the Joaquin center was well within a region of moderate VWS-C. These VWS-C changes may have created a more "favorable" area of VWS-C to the west of the center of Joaquin before the track reversal (Figure 12, upper right). It is uncertain whether the shifts of the very small VWS-C centers from the west to the north of the center (Figure 12, lower right) is a cause or an effect of the steering Joaquin around the bottom of the loop instead of a continuation of the track to the west-southwestward. Further study is necessary to understand if these the horizontal shifts of the very small VWS-C contributed to the track reversal of Joaquin.

In addition to the area-average moderate (or lower, as in Figure 12) VWS-C value of 8 m s^{-1} (Table 2, row 2), another possible contribution to the continued RI during Segment B may have been ocean heat content (OHC) values above 50 kJ cm^{-2} that are considered to be favorable for TC formation and intensification (NOAA, RAMMB). For example, the OHC at 0000 UTC 1 October near the mid-time of Segment B is between 50 - 75 kJ cm^{-2}, which would be favorable for intensification (Figure 13). Note that forecast track positions (grey hurricane symbols from 0 h to 120 h) are not correct, as the actual position of Joaquin was at 23.1 N, 73.7 W at 1200 UTC 1 October, which is 12 h after the initial position in Figure 13 (Table 3, row 2). Subsequently, Joaquin was at 22.9 N, 74.4 W at 0000 UTC 2 October (Table 2, row 3), and 23.3 N, 74.8 W at 1200 UTC 2 October (Table 3, row 4). The differences in latitude and longitude between the NHC best-track positions and the 72 h NHC official track forecast are listed in Table 3. Note that latitude

(longitude) difference after 72 h is 4.2 deg (5.2 deg), so caution is advised in interpreting the track in Figure 13. However, the actual track of Joaquin (not shown) was over OHC > 50 kJ cm^{-2} for about 36 h according to this RAMMB analysis (Figure 13).

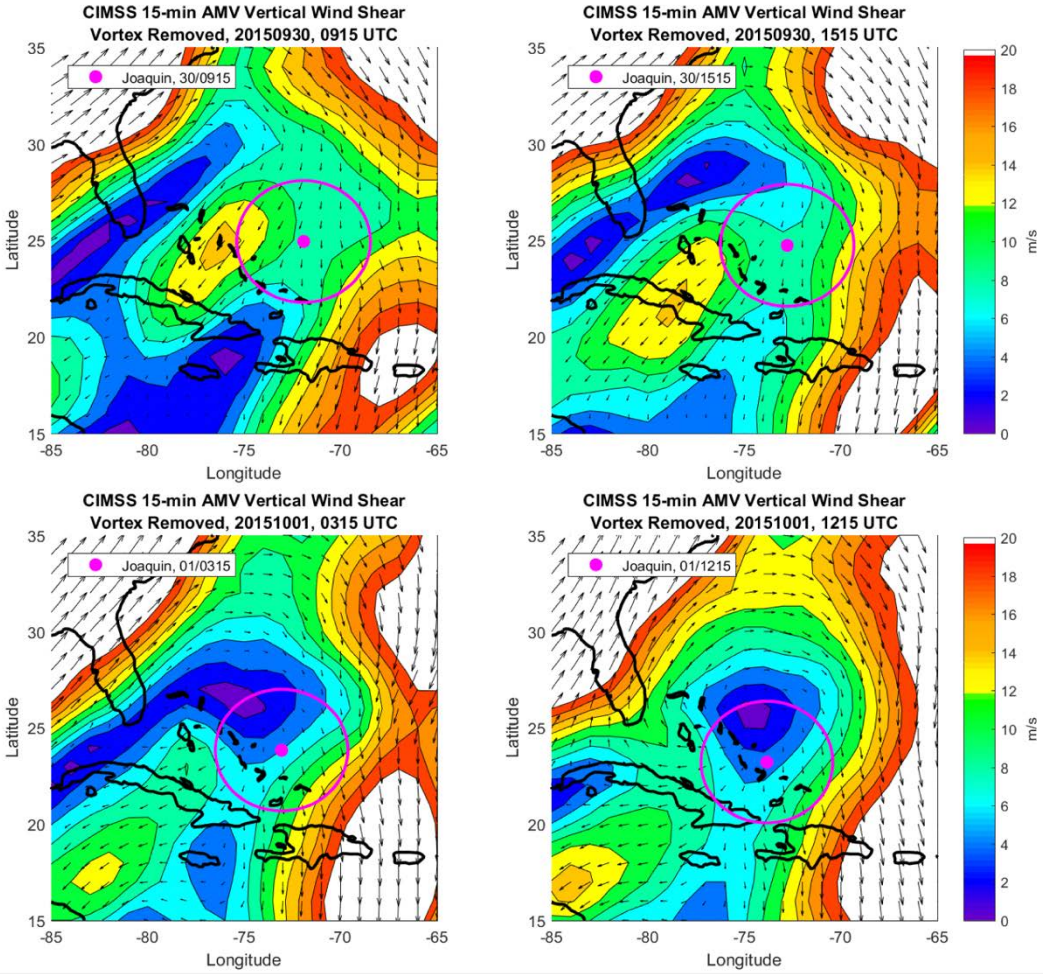

Horizontal plots of the VWS-C vectors relative to the SATCON position of Joaquin (magenta dot) during the rapid VWS direction change. The VWS-C values in Figure 9 and Table 2 are averaged over the circle with a radius of 350 km (upper left) 0915 UTC 30 September, (upper right) 1515 UTC 30 September, (lower left) 0315 UTC 1 October, and (lower right) 1215 UTC 1 October.

Figure 12. CIMSS VWS vector field during rapid VWS direction change

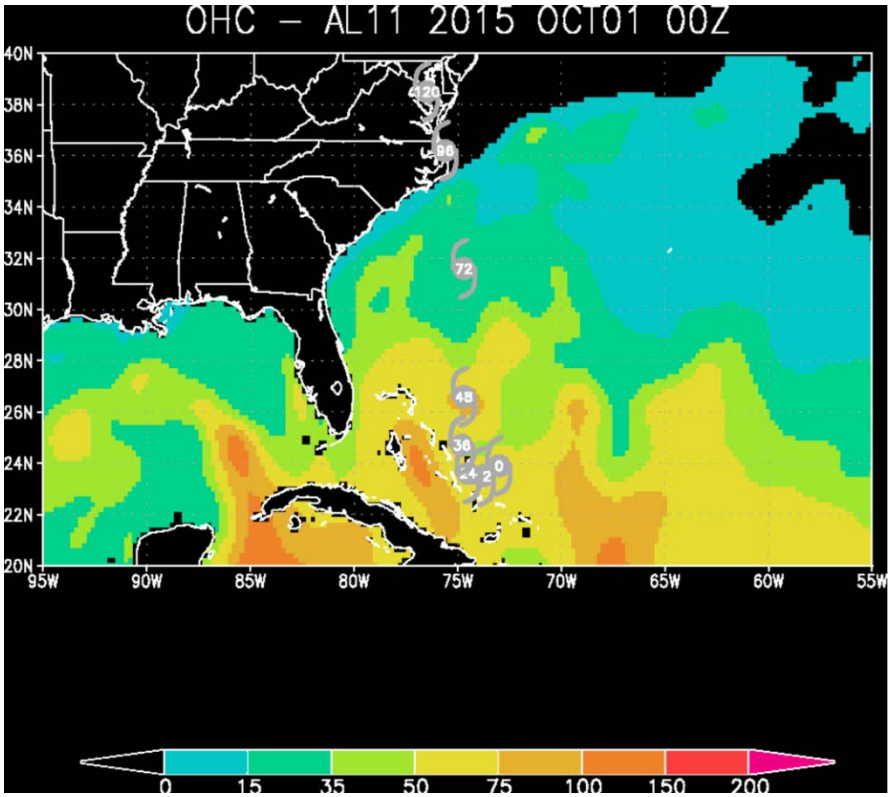

Spatial grid spacing is 0.2 x 0.2 lat/long with units of kJ cm^{-2}. Grey hurricane symbols from initial time t = 0 to 120 h are for NHC forecast track and are not correct.

Figure 13. Tropical cyclone ocean heat content (OHC) for Hurricane Joaquin 0000 UTC 1 October. Source: NOAA Satellites and Information, Regional and Mesoscale Meteorology Branch (RAMMB) (Accessed: 21 February 2019).

Table 3. NHC best-track versus NHC forecast track from 0000 UTC 1 October. Source: NOAA Satellites and Information, Regional and Mesoscale Meteorology Branch (RAMMB) (Accessed: 21 February 2019).

Forecast Hour	NHC Best Track Lat	NHC Forecast Lat	NHC Best Track Lon	NHC Forecast Lon	Diff. in Best track / forecast Lat	Diff in Best track / forecast Lon
0	23.9	23.9	-73	-73	0.0	0.0
12	23.1	23.5	-73.7	-73.8	0.4	0.1
24	22.9	23.6	-74.4	-74.5	0.7	0.1
36	23.3	24.7	-74.8	-74.8	1.4	0.0
48	25.6	26.6	-72.6	-74.7	1.0	2.1
72	27.4	31.6	-69.5	-74.7	4.2	5.2

Differences between the NHC best-track latitudes and longitudes versus the 72-h NHC official track forecast from 0000 UTC 1 October 2015 shown in Figure 13. Data for NHC forecast track source: NOAA Satellites and Information. Data for NHC best-track data source: Berg (2016).

3. Segment C and Event II: Track Reversal and Pre-rapid Intensification

Even though the VWS-C here is being categorized as low at an average value of -2.6 m s^{-1} below moderate VWS of 8 m s^{-1} for Segment C (Table 2, row 3), Joaquin had a decreasing trend of intensity change averaging 0.96 kt for this short segment (Table 2, row 3). According to Berg (2016), this was the time that Joaquin made landfall over the Bahamas, and thus Joaquin most likely weakened due to interactions with the islands. Whereas the interaction with land may have contributed to the weakening, the slow movement over the warm ocean may have led to enhanced mixing at the base of the ocean mixed layer, or even some cooling due to upwelling in shallow water. Nevertheless, Joaquin started to intensify 6 to 12 h after the low VWS-C, which likely did contribute to setting up a favorable environment for Joaquin's second RI (Event III). As will be described below, the second RI did not happen immediately after encountering the favorable environment as did the first RI event.

Horizontal plots of the VWS-C vectors at 0615 UTC 2 October and 1215 UTC 2 October in Figure 14 do indicate a shift in the VWS field northwest of Joaquin during the timeframe of the track reversal. A region of small (5 m s^{-1}) VWS-C (averaged over a 350 km radius) surrounds Joaquin at 0615 UTC, but by 1215 UTC a region of larger VWS-C has encroached upon the center of Joaquin from the east. While this increase in VWS-C is also evident in Figure 9, the area-average VWS-C is just into the range of moderate VWS (~8 m s^{-1}), and these VWS-C values continue in the moderate range until after the second RI is in progress. Berg (2016) attributes the VWS change to a breakdown of the high pressure over the southeastern United States. By contrast, the plots of VWS-C vectors between 0615 UTC and 1215 UTC 2 October in Figure 14 indicate that the smaller VWS-C are because Joaquin is in a null region between large VWS-C associated with the upper troposphere troughs to the east and to the west. In this situation, the increase in the area-average VWS-C may be associated with the eastern trough moving closer to Joaquin or vice-versa.

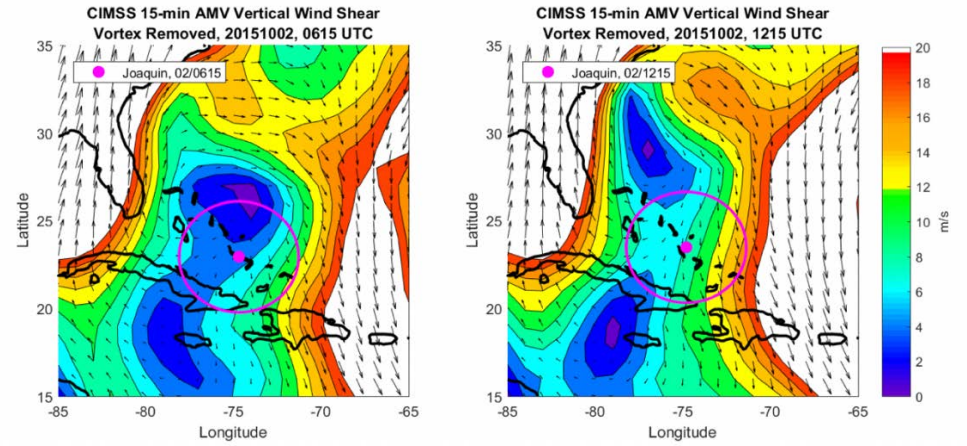

Horizontal plots of the VWS-C vectors relative to the SATCON position of Joaquin (magenta dot) at (left) 0615 UTC and (right) 1215 UTC 2 October during the track reversal. The VWS-C values in Figure 9 and Table 2 are averaged over the circle with a radius of 350 km.

Figure 14. CIMSS VWS field during the track reversal event

It is important to note that the VWS-C is not uniform around the storm, and this lack of symmetry in the VWS-C relative to the Joaquin center could have a connection to the track reversal. As Joaquin reversed direction around the loop, the anticyclone outflow aloft that is streaming to the south may be at lower elevation in the upper troposphere because Joaquin has been weakened. Furthermore, the weaker outflow may not have been spiraling out to the east as far before turning to the south. This scenario may indicate that the outflow is joining the trough to the east. In Figure 14 (left) at 0615 UTC 2 October, there is encroachment of higher VWS-C from the right of the magenta circle to closer to the center of the storm that was not present in Figure 14 (right) only 6 h later at 1215 UTC 2 October. An area of higher VWS-C that is centered around 70 W in Figure 14 (left) has penetrated westward to be centered around 72 W in Figure 14 (right). In this line of reasoning, the encroachment of the larger VWS-C from the east would be a result of the track reversal rather than a cause. Even though the vortex is removed in the VWS-C, if the Joaquin outflow has joined with the trough, the VWS-C horizontal plot would show a larger VWS-C to the east of Joaquin's center. Thus, the VWS-C shifts are not a contributing factor, but rather a result of the new translation direction of Joaquin.

During the short Event II at 0900 UTC to 1500 UTC 2 October, Joaquin has passed through the southernmost point in the track reversal and now has a storm heading of ~180

deg from the south (Figure 9). Even though the VWS-C magnitude has increased to just 0.12 m s^{-1} below the moderate 8 m s^{-1} VWS, the average intensity change per 6 h is -3.6 kt (Table 2, row 6). As indicated above, it seems counter-intuitive that a hurricane with an intensity of 120 kt (NHC) or 112 kt (SATCON) at 0900 UTC 2 October would have a decrease in intensity with just a small increase in VWS-C back into the middle of the moderate range.

During Event II, the OHC is almost 75 kJ cm^{-2} (Figure 15), which should have been favorable for intensification. As in the case of Figure 13, the reader is cautioned to disregard the NHC official track forecast after 36 h in Figure 15 (grey TC symbols). The NHC best-track and the official track forecast are compared in Table 4. Note that after 36 h, the official track forecast deviates from the best-track by large magnitudes.

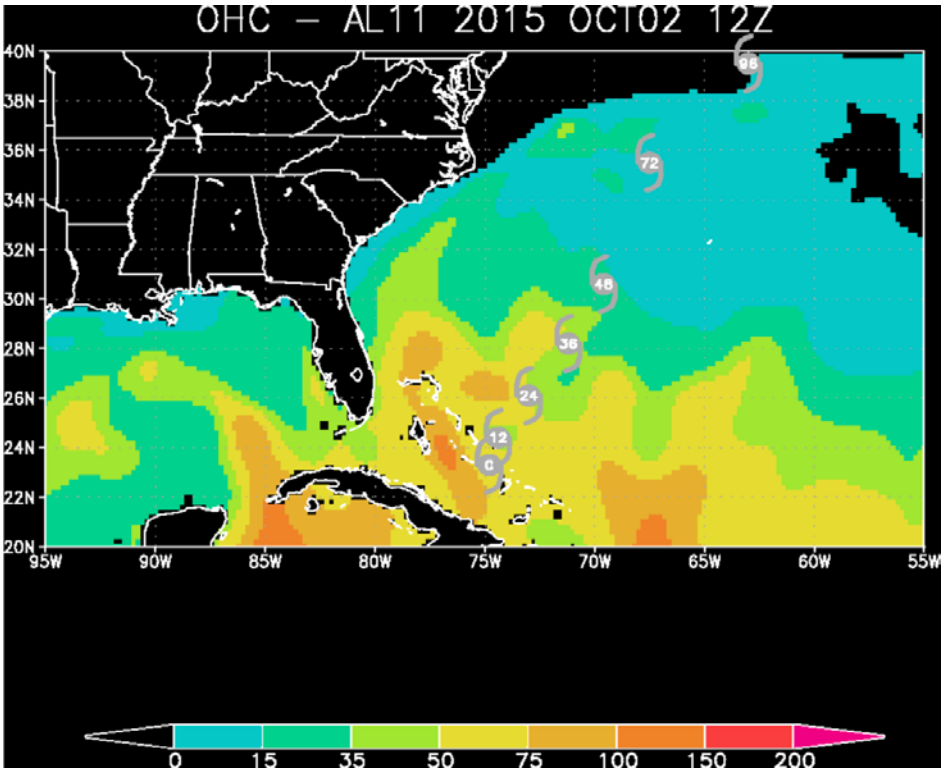

Spatial grid spacing is 0.2 x 0.2 lat/long with units of kJ cm^{-2}. Grey hurricane symbols from time = 0 to 96 h are the NHC official track forecast and are not correct.

Figure 15. Tropical cyclone ocean heat content (OHC) for Hurricane Joaquin 1200 UTC 2 October. Source: NOAA Satellites and Information, Regional and Mesoscale Meteorology Branch (RAMMB) (Accessed: 21 February 2019).

Table 4. NHC best-track versus NHC forecast 1200 UTC 2 October. Source: NOAA Satellites and Information, Regional and Mesoscale Meteorology Branch (RAMMB) (Accessed: 21 February 2019).

Forecast Hour	NHC Best Track Lat	NHC Forecast Lat	NHC Best Track Lon	NHC Forecast Lon	Diff. in Best track / forecast Lat	Diff in Best track / forecast Lon
0	23.3	23.3	-74.8	-74.8	0.0	0.0
12	23.9	24.4	-74.8	-74.4	0.5	0.4
24	25.6	26.1	-72.6	-73.0	0.5	0.4
36	27.4	28.2	-69.5	-71.2	0.8	1.7
48	30.4	30.6	-67.1	-69.6	1.2	2.5
72	32.6	35.5	-65.8	-67.5	2.9	1.7

Differences between the NHC best-track latitudes and longitudes versus the 72-h NHC official track forecast from 1200 UTC 2 October 2015 shown in Figure 15. Data for NHC forecast track source: NOAA Satellites and Information. Data for NHC best-track data source: Berg (2016).

It is important to note that Event II has a negative intensity change with an average of -3.6 kt in an environment with a VWS-C average of 7.88 m s^{-1} with a correlation coefficient of -1.0 (Table 2, row 6). However, Joaquin starts the second RI (Event III) almost simultaneously as the VWS-C increases at 2100 UTC 2 October to an average value of 9.36 m s^{-1} (Table 2, row 7). It is possible that these early large OHC values during Event II contributed to the second RI later during Event III.

An alternative to environmental VWS being responsible for the decreasing intensities during Event II is the ocean feedback to the Joaquin wind forcing. Early in Event II, Joaquin was slowly moving poleward for 12 h and then more rapidly toward the north-northeast. Obscured by the 12 h grey symbol in Figure 15 is an OHC region with values <50 kJ cm^{-2}. As discussed before, values < 50 kJ cm^{-2} would lead to a decrease in intensity in a TC. In Figure 15, the obscured region of 35-50 kJ cm^{-2} OHC values is to the east of Joaquin's northeastward track after the track reversal. The area of lower OHC is actually located from 24 N to 25 N, 75 W to 72 W, and Joaquin's actual track was just west of the lower OHC values along 74.8 W.

An alternate explanation of how lower OHC could have affected Joaquin's intensity is summarized in a conceptual model of ocean cooling effects during the looping track reversal of Joaquin (Figure 16). At storm translation speeds above ~ 3 m s^{-1}, the ocean cooling is mostly due to mixing processes and the combination of the vortex wind structure plus (or minus) the translation speed leads to stronger (or weaker) mixing processes on the right (or left) of the path in the Northern Hemisphere. Since the track reversal of Joaquin was an anticyclone loop (Figure 8), if the ocean cooling was primarily due to mixing processes then the ocean region within the loop would have experienced larger cooling both during the southwestward track segment and the northeastward segment (Figure 16a, dashed lines within the track). This ocean-cooled air would not have been present at the starting location of Joaquin but would have been generated by Joaquin as it tracked southwestward and then northeastward.

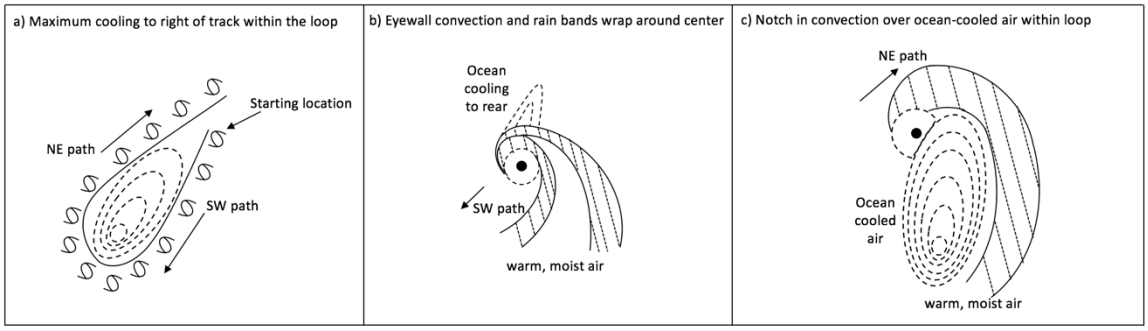

Conceptual model of the ocean mixing effects during the looping track of Joaquin (panel a). Eyewall convection and rain bands wrapping around center during southwestward track (panel b) and notch in convection over ocean-cooled water on northeastward track (panel c). Highly asymmetric deep convection diabatic heating will tend to introduce cross-track deflection away from the maximum ocean cooling on both southwestward and northeastward paths.

Figure 16. Ocean cooling effects on Hurricane Joaquin.

Satellite images during each phase of the Joaquin track loop (Figure 17) were analyzed to validate the above conceptual model. Due to the north-to-south air temperature and moisture gradient, the low-level inflow into Joaquin during the southwestward path would bring more warm and moist air into the eastern semi-circle and more cool and dry air into the western semi-circle (Figure 16b). During the Joaquin southwestward track, and during the loop, this contrast in enthalpy (sensible heat and latent heat) fluxes between the

eastern and western semicircles would be further enhanced by the maximum ocean cooling to the right side of the path. In enhanced infrared satellite imagery at 1715 UTC 1 October (Figure 17, upper left) when Joaquin was near the end of its southwestward path (Figure 8), the deep convection pattern is similar to the classic hurricane pattern as depicted in the diagram in Figure 16b. There is some asymmetry with broader deep convection to the southeast of the center (band of yellow just southeast of the eye) that may be attributed to warmer, more moist air flow from the south is being injected into the storm. The narrow band of deep convection is the western semi-circle which would be to the west of the ocean cooled air in the conceptual model (Figure 16b).

During the northeastward path, the eastern semi-circle of Joaquin is hypothesized to have a markedly reduced enthalpy flux over the ocean-cooled air (Figure 16c). If the source of warm, moist air for the maintenance of Joaquin is from the south, the deep convection will necessarily be displaced to the east of the ocean-cooled region. Consequently, there is a "notch" in the deep convection (Figure 17, lower right) that will exist over the ocean-cooled region, which is represented as a region of green around ~22 N, 75 W that is penetrating into the asymmetric red convective area around the eye. Another effect of the reduced enthalpy flux due to the greater ocean cooling on the right side of the anticyclone looping track reversal of Joaquin would be decreasing intensity along the northeastward track segment until Joaquin was beyond the ocean cooled air (Figure 16). Therefore, the asymmetric deep convection in relation to the ocean-cooled region associated with the track loop is hypothesized to explain the lack of intensification during Event II despite relatively low VWS-C and overall high OHC in the region of the Bahamas.

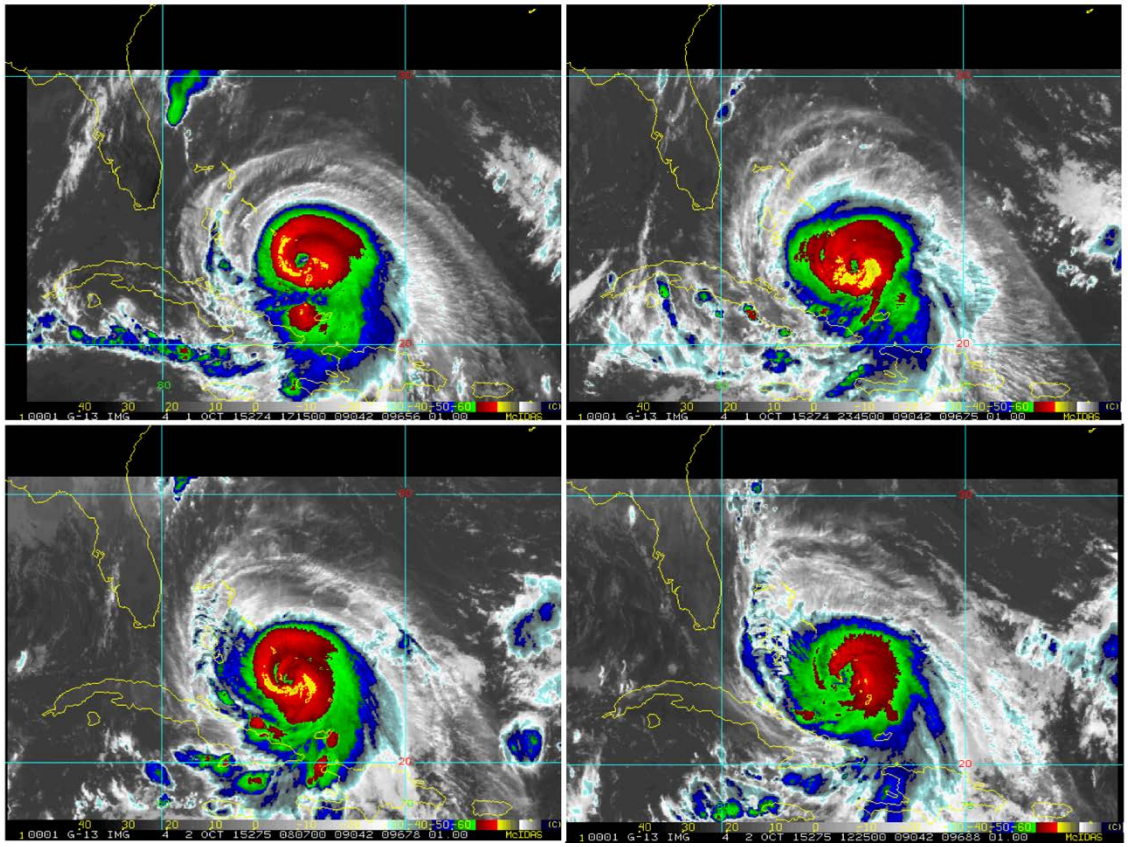

Remapped infrared imagery (~11 μm) at 4 km resolution taken from geostationary satellites (GOES-East) at (upper left) 1715 UTC 1 October, (upper right) 2345 UTC 1 October, (lower left) 0807 UTC 2 October, and (lower right) 1225 UTC 2 October 2015.

Figure 17. Enhanced IR satellite image showing the evolution of a notch in Joaquin. Source: NOAA Satellites and Information, Regional and Mesoscale Meteorology Branch (RAMMB) (Accessed: 05 March 2019).

Since the track reversal may be related to the deep convection pattern change hypothesized between Figure 16b and Figure 16c, the evolution of the deep convection during the loop is indicated in the other three panels in Figure 17. Recall that prior to the track reversal at 1715 UTC 1 October (Figure 17, upper left), a well-organized curved outer rain band (curved yellow region around the eye) to the west of the center spiraled into the southern quadrant of a fairly large eyewall. However, there was no similar rain band to the northeast of the eye region either in the eyewall or in the outer rain band, which may be

attributed to the ocean cooling that occurred behind the center along the southwestward track. The area of smaller OHC at 0000 UTC 1 October is near 24.5 N, 74 W (Figure 13), while the center of Joaquin is located at ~24 N, 75 W (Figure 17, upper left). The lower OHC area is therefore slightly northeast of the position of Joaquin, which is coincident with the first panel of the conceptual model when they cyclone is at its southernmost point.

At the bottom of the loop in the Joaquin track reversal around 2345 UTC 1 October (Figure 17, upper right), deep convection was present in a broad radial region within the southern semi-circle, but none in the northern semi-circle. A broad cyclonically curved rain band is in the southeast quadrant (yellow band directly south of the eye), but it does not encircle the eye when Joaquin was at the bottom of the loop. Perhaps this absence of deep convection may be attributed to the ocean-cooled region that is expected to be a maximum just to the northeast of the eye at the bottom of the loop (see Figure 16a). Such an asymmetric diabatic heating distribution (warming to south compared to the north) may have also contributed to the track of Joaquin drifting to the south away from the ocean-cooled region as it turned around the bottom of the loop.

Just 8.5 h later at 0807 UTC 2 October (Figure 17, lower left), the deep convection had fully wrapped around the eye (yellow band fully circling around the eye), and the broad curved rain band to the southeast of the eyewall has shrunk in size from the upper-right image. A narrow cyclonically curved rain band is now present in the southern semi-circle, but it passes to the south of the eye to join the residual rain band to the southeast of the eye. The wrapping around of the narrow-curved rain band to the east of the ocean-cooled region is considered to be the start of the notch in the deep convection in the conceptual model in Figure 16c, because only 4.5 h later at 1225 UTC 2 October (Figure 17, lower right), the notch was fully present. Whereas, the colder water as in the conceptual model at 1200 UTC 2 October was located at 24 N to 25 N, 73 W to 75 W, the center of Joaquin was near 23.5 N, 74.8 W at 1225 UTC 2 October (Figure 18). Thus, Joaquin's position is west of the smaller OHC, which again consistent with the conceptual model. Interestingly, 1200 UTC 2 October was one time at which the NHC best-track and SATCON positions were identical in Figure 8. At this time Joaquin had just passed the bottom of the loop and the

open eye was represented by a curved inner eyewall cloud in Figure 18, which is better visualized as an enlarged version of Figure 17 (lower right).

In addition to being a partial demonstration of the ocean cooling effects on the Joaquin intensity changes hypothesized in the conceptual model in Figure 16c, the 20 h sequence of satellite imagery in Figure 17 suggests vortex structure changes that may have had a role in the Joaquin track reversal. Berg (2016) described a synoptic situation at this time of Joaquin as high pressure to the northwest of Joaquin's path and lower pressure to the southeast of Joaquin's path. Specifically, the mid-tropospheric pressures associated with the steering flow during the southwestward path would be higher to the northwest and lower to the southeast. As the southwestward path was coming to an end, the Joaquin deep convection pattern suggests a classical hurricane vortex structure with an eyewall (Figure 17, upper left). Even after 6.5 h (Figure 17, upper right) and 15 h later (Figure 17, lower left), there was a partially closed eyewall deep convection. By this time, the steering flow was associated with high (low) pressure to the north (south), but this pressure gradient was weak as Joaquin was moving slowly westward (Berg 2016).

As Joaquin passed the bottom of the loop, the satellite imagery (Figure 17, lower right) indicated no deep convection near the center, and both the NHC best-track and the SATCON intensity estimate indicate the Joaquin intensity was decreasing. Hendricks et al. (2018, Figure 5a) documented that 6 h later the vortex center could not be clearly defined above 11.5 km, rather than extending higher in the upper troposphere. Meanwhile, the cluster of deep convection at 1225 UTC 2 October (Figure 18) was well to the south-southeast of the center, and to the east of the ocean cooled air. As previously stated, the ocean-cooling is to the east of Joaquin at this time. If the conceptual model is correct, there should be a "gap" in the deep convection directly south of the eye with deeper convection farther east (Figure 16c). This is evident in Figure 18 where the red band of deep convection at ~22 N and south-southeast of the center of Joaquin does not extend fully around to the south and southwest of the storm as with typical TC structures. Thus, at a time that Joaquin was in a weak steering flow with low pressure to the south and higher pressure to the north, the diabatic heating associated with the cluster of deep convection was tending to decrease the lower-tropospheric pressures to the southeast.

A hypothesis to be tested in the future is whether the pressure decrease to the southeast would be sufficient to change the steering flow such that Joaquin came out of the bottom of the loop with a northeastward path, rather than a northwestward path toward the east coast of the United States as most of the numerical models had predicted (Figure 2). In order to correctly predict this diabatic heating modification of the steering flow pressure gradient, the model must predict the notch in the deep convection in relation to the Joaquin center and the ocean cooled air as in Figure 16c.

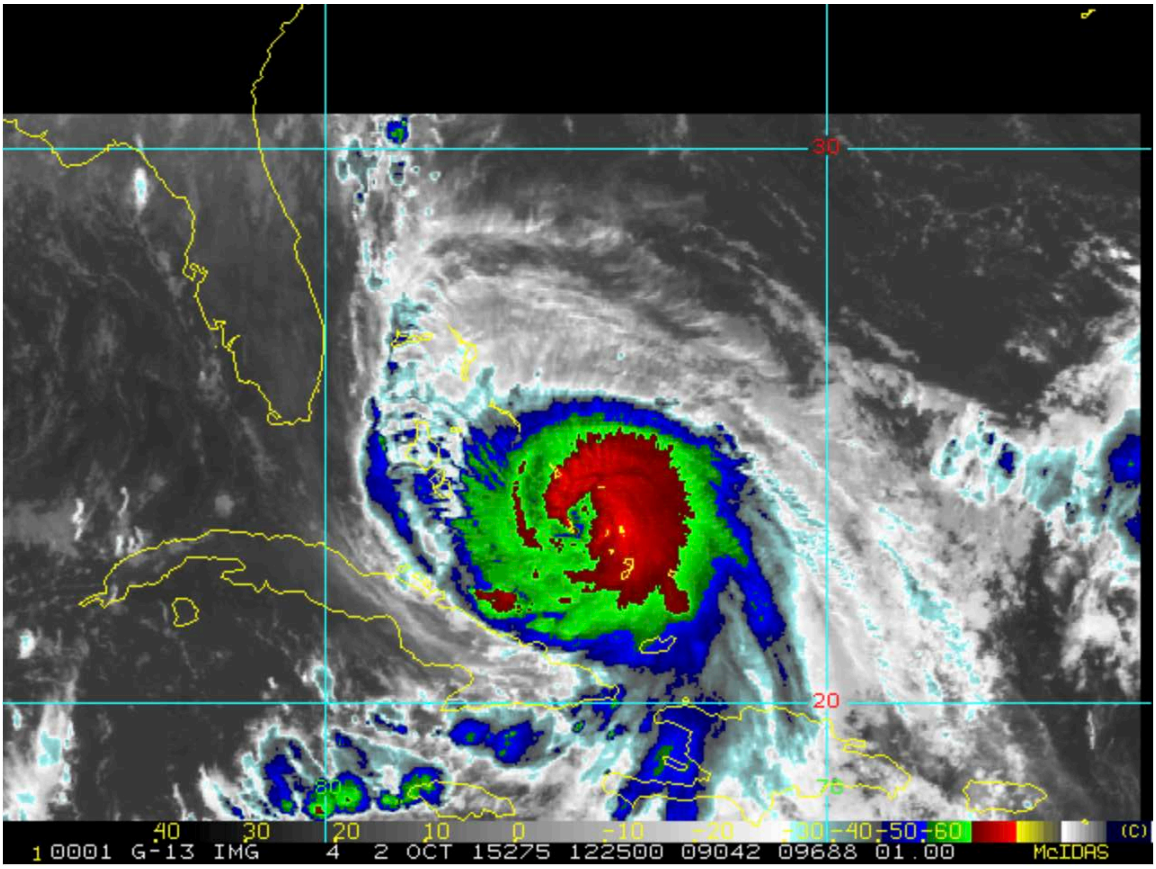

Remapped infrared imagery (~11 μm) at 4 km resolution taken from geostationary satellites (GOES-East) at 1225 UTC 2 October 2015, which is less than 6 h after Joaquin had crossed around the bottom of the loop in the track reversal.

Figure 18. Enhanced IR satellite picture of Joaquin 1225 UTC 2 October. Source: NOAA Satellites and Information, Regional and Mesoscale Meteorology Branch (RAMMB) (Accessed: 05 March 2019).

4. Event III: Rapid Intensification in High VWS

Event III is the second RI event of Joaquin, which began at 2100 UTC 2 October and peaked at 0900 UTC 3 October (Figure 9). Averaged over this 12 h interval, the intensity change per 6 h was only 7.4 kt because early in the interval the intensity changes were relatively small. Before the second RI event, a representative VWS value of 8 m s^{-1} can be used for the period between 0600 UTC 2 October and 1800 UTC 2 October (Figure 9). At 1800 UTC October, the VWS decreases below moderate VWS to 7 m s^{-1}. This -1 m s^{-1} shift correlates with a change from a negative intensity change (representative value of -3 kt per 6 h) to positive intensity change (representative value of +2 kt per 6 h). The slight VWS decrease and small intensity increase are negatively correlated. However, Joaquin's second RI event becomes readily apparent at 0000 UTC 3 October with a large intensity increase to a maximum of 18 kt per 6 h. At 1325 UTC 3 October, which is about one hour after Joaquin attained peak intensity, the deep convection in the eye wall has almost completely wrapped around the eye of Joaquin (Figure 19). Therefore, as Joaquin has moved northeastward beyond the region of maximum ocean cooling in Figure 16a the ocean response of adding warm, moist air to the system can now contribute to the second RI event.

A counter-intuitive aspect of the second RI Event III is that it began during a period of moderate VWS, but the VWS-C then increased to a maximum value of ~ 13 m s^{-1} (Figure 9) during the same 6-h interval as the intensity change per 6 h has a value of ~ 15 kt. The moderate VWS-C at 1945 UTC 2 October just prior to the beginning of the second RI was because Joaquin was between a large southward-oriented VWS region to the east and a large northward-oriented VWS to the west associated with an approaching trough over the southeast United States (Figure 20, left). This approaching trough and associated upper-tropospheric winds may have contributed to the initiation of a second outflow jet to the north near ~28 N, 72 W (Figure 19). However, the dominant outflow is toward the southeast on the eastern side of the center, and this is already reflected in the outward angle of the VWS-C vectors in Figure 20 (left). At 0915 UTC 3 October when the peak RI intensity change was occurring, the VWS-C vector field is highly asymmetric (Figure 20, right). While there is a region of VWS-C values greater than 20 m s^{-1} to the east of the

center (Figure 20, right) that is clearly related to the outflow near ~22 N to 28 N, 68 W (Figure 19), there is VWS-C across the center that appears to be associated with a cyclonic vortex near 32 N, 67 W (Figure 20, right). Since the VWS-C vectors in the tropics and subtropics are closely related to the upper-tropospheric winds (including therefore outflow direction and magnitude), these higher wind speeds in the upper atmosphere will dominate the vector direction in the horizontal VWS plots utilized in this thesis. Averaged over the circle of radius 350 km, the VWS-C is ~ 13 m s^{-1}, which is then 5 m s^{-1} over the moderate value (~8 m s^{-1}). Based on these VWS-C vectors, it appears that the second RI of Joaquin could occur simultaneously with large VWS-C values due to a favorable interaction with an adjacent upper-troposphere trough that enhanced the outflow.

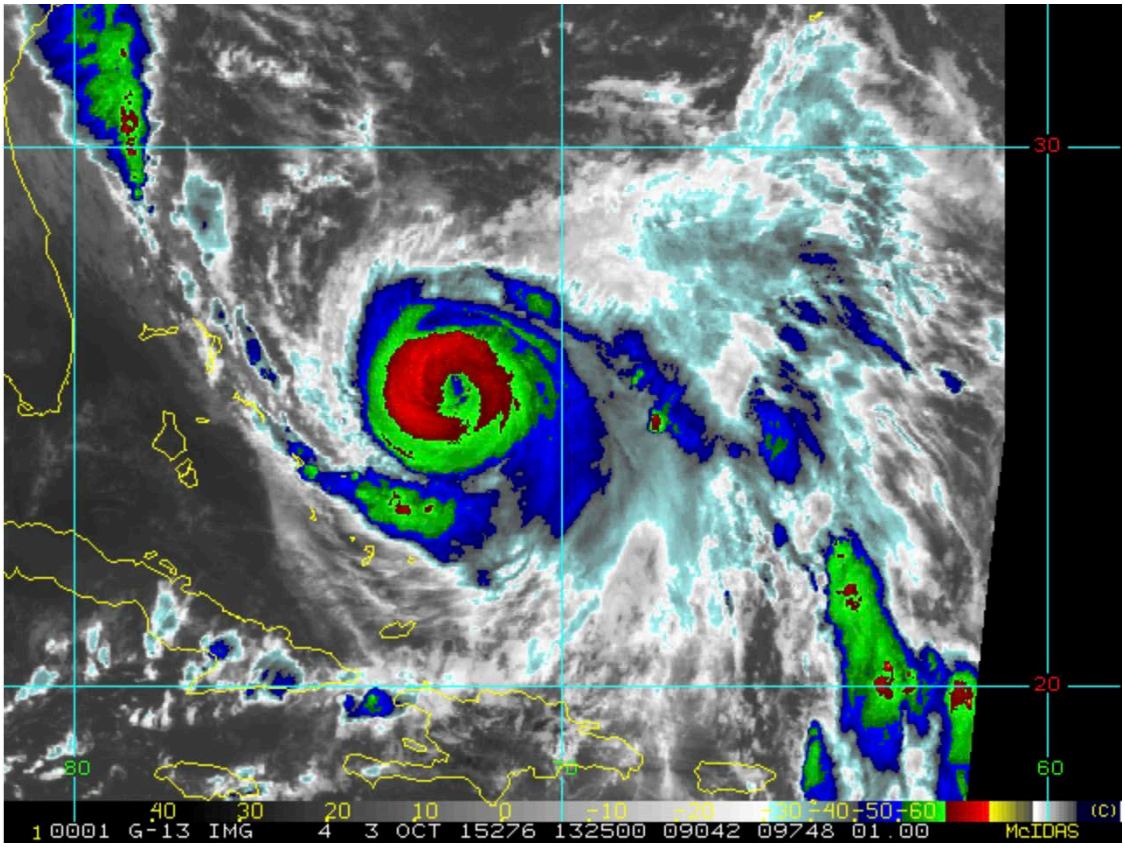

Remapped infrared imagery (~11 μm) at 4 km resolution taken from geostationary satellites (GOES-East) at 1325 UTC 3 October 2015, which is only an hour after Joaquin attained peak intensity after the second RI event.

Figure 19. Enhanced IR satellite picture of Joaquin 1325 UTC 3 October. Source: NOAA Satellites and Information, Regional and Mesoscale Meteorology Branch (RAMMB) (Accessed: 05 March 2019).

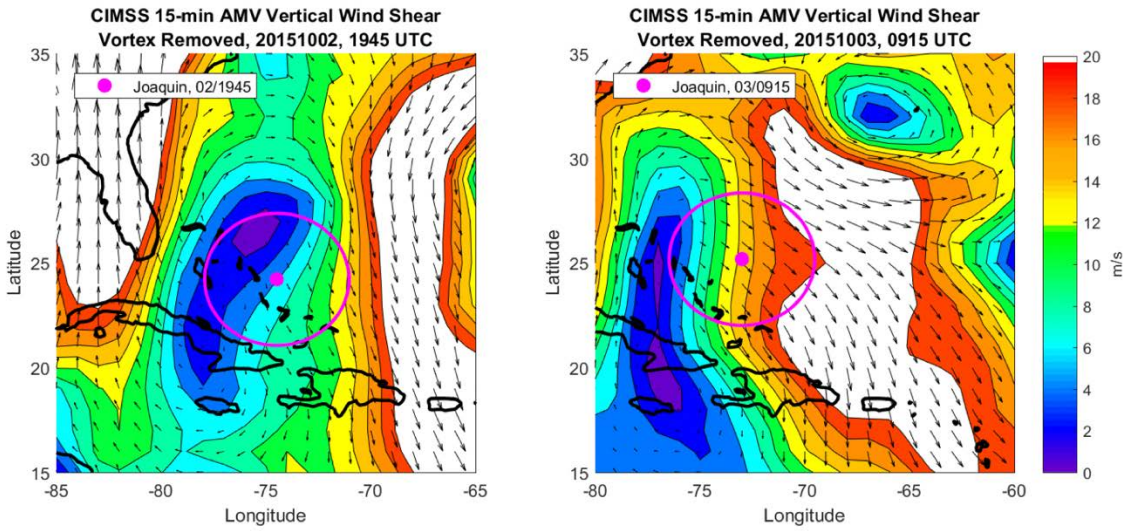

Horizontal plots of the VWS-C vectors relative to the position of Joaquin (magenta dot) at (left) 1945 UTC 2 October and (right) 0915 UTC 3 October during the second RI. The VWS-C values in Figure 9 and Table 2 are averaged over the circle with a radius of 350 km.

Figure 20. CIMSS VWS fields near peak time of second RI

The correlation of VWS-C magnitude deviations from a moderate 8 m s^{-1} value and intensity change during Event III is surprisingly positive at a value of 1.0 (Table 2, row 7), which suggests that the rapid intensity increase was at least coincident, or perhaps actually leads the VWS-C increase. The difference between the VWS-C (313 deg) heading and the storm heading (228 deg) is 085 deg. It was the track reversal 12 h prior to the start of the second RI event that led to this 085 deg difference in heading. Perhaps coincidentally, it was approximately 12 h before Joaquin's first RI event that the VWS heading and storm heading were also less than 90 deg apart (~ 70 deg) (Figure 9). Additional study is necessary to understand how this smaller difference between VWS direction and storm heading may have contributed to Joaquin rapidly intensifying despite the large magnitude of VWS-C.

5. Event IV and Segment D: Rapid Decay and Interrupted Decay

Elsberry et al. (2018) and Hendricks et al. (2018) have extensively examined the Event IV of Joaquin, which was characterized by extremely rapid decay and then an abrupt interruption in that decay, which is labeled as Segment D in Table 2. At the beginning of Event IV (1500 UTC 3 October), Joaquin was moving north-northeastward and was undergoing rapid decay in response to large (17 m s^{-1}) VWS-C (Figure 9). Over the 12 h Event IV, the average intensity change per 6 h was -8.9 kt under the influence of an average VWS-C of 12.27 m s^{-1} (Table 2, row 8), and thus the correlation coefficient was -0.4.

In the RAMMB analysis (Figure 21), a region of lower OHC values is analyzed along the northeastward storm track from 1200 UTC 3 October to 0000 UTC 4 October according to the NHC forecast at 1200 UTC 3 October. While this NHC predicted track is off 0.4 deg latitude and 0.7 deg longitude from the NHC best-track (Table 5, row 2), this southwestward shift of the grey 12 h hurricane symbols would still indicate that Joaquin would be passing over a region of minimum OHC already in the first 12 h. Clearly after 12 h, Joaquin would be rapidly moving north-northeastward over OHC < 50 kJ cm^{-2}, which would be expected to contribute to the observed rapid decay of Joaquin. It should be noted that the minimum region along the 0-12 h track in Figure 21 should not be confused with the ocean cooled region in the conceptual model (Figure 16c). As described in Section 3, Joaquin had rapidly intensified along the northeastward path after leaving the ocean cooled region.

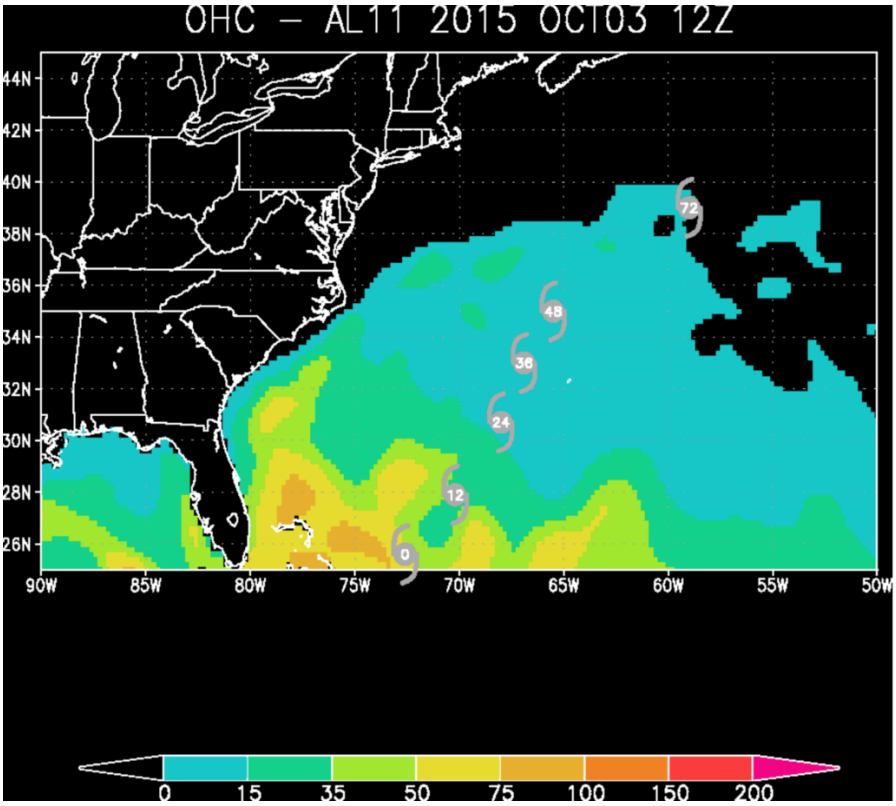

Spatial grid spacing is 0.2 x 0.2 lat/long with units of kJ cm^{-2}. Grey hurricane symbol for the forecast track is not correct.

Figure 21. Tropical cyclone ocean heat content (OHC) for Hurricane Joaquin 1200 UTC 3 October. Source: NOAA Satellites and Information, Regional and Mesoscale Meteorology Branch (RAMMB) (Accessed: 21 February 2019).

Table 5. NHC best-track versus NHC forecast from 1200 UTC 3 October. Source: NOAA Satellites and Information, Regional and Mesoscale Meteorology Branch (RAMMB) (Accessed: 21 February 2019).

Forecast Hour	NHC Best Track Lat	NHC Forecast Lat	NHC Best Track Lon	NHC Forecast Lon	Diff. in Best track / forecast Lat	Diff in Best track / forecast Lon
0	25.6	25.6	-72.6	-72.6	0.0	0.0
12	27.4	27.9	-69.5	-70.2	0.4	0.7
24	30.4	30.7	-67.1	-68.0	0.3	0.9
36	32.6	33.0	-65.8	-66.9	0.4	1.1
48	34.6	35.0	-64.9	-65.5	0.4	0.6
72	36.4	39.0	-63.4	-59.0	2.6	4.4

Differences between the NHC best-track latitudes and longitudes versus the 72-h NHC official track forecast from 1200 UTC 3 October 2015 shown in Figure 19. Data for NHC forecast track source: NOAA Satellites and Information. Data for NHC best-track data source: Berg (2016).

Even at the interruption of decay on 0000 UTC 5 October according to the NHC best track (Figure 6), Joaquin was in the low to moderate VWS-C of ~7 m s^{-1} (Figure 9). According to the SATCON intensity estimates, the decay continued another 6 h and then oscillated between weak intensification and weak decay (Figure 9). That is, the VWS-C continued to decrease to ~5 m s^{-1} at 0900 UTC 5 October, and then returned to the moderate VWS range (~8 m s^{-1}) around 1500 UTC 6 October. Averaged over Segment D, Joaquin had a slight positive intensity change (0.77 kt / 6 h) while in moderate VWS-C equal to 6.9 m s^{-1} (Table 2, row 4). Thus, the correlation coefficient was a positive (not negative) 0.19 overall during Segment D, since the SATCON intensity change was increasing when the VWS-C was below the moderate definition, which is another example of nonlinear behavior during Joaquin. By contrast, the correlation coefficient between the NHC best-track intensity changes and VWS-S would be 0.0 (Figure 6) since the NHC intensities were constant at 75 kt for 30 h during Segment D.

There are two times in Segment D when Joaquin intensified immediately after the VWS-C and storm heading were very close in direction (Figure 8). The first time was after 1800 UTC 4 October when the VWS-C heading and the storm heading were within 40 deg (VWS-C from the west and storm heading from the southwest), and the second time was after 1500 UTC 6 October when the VWS-C and storm heading were almost the same (VWS-C from the west and storm heading from the west). At the first time, Joaquin's intensity increase was almost 15 kt / 6 h, and at the second time Joaquin's intensity increase was almost 10 kt / 6 h (Figure 9).

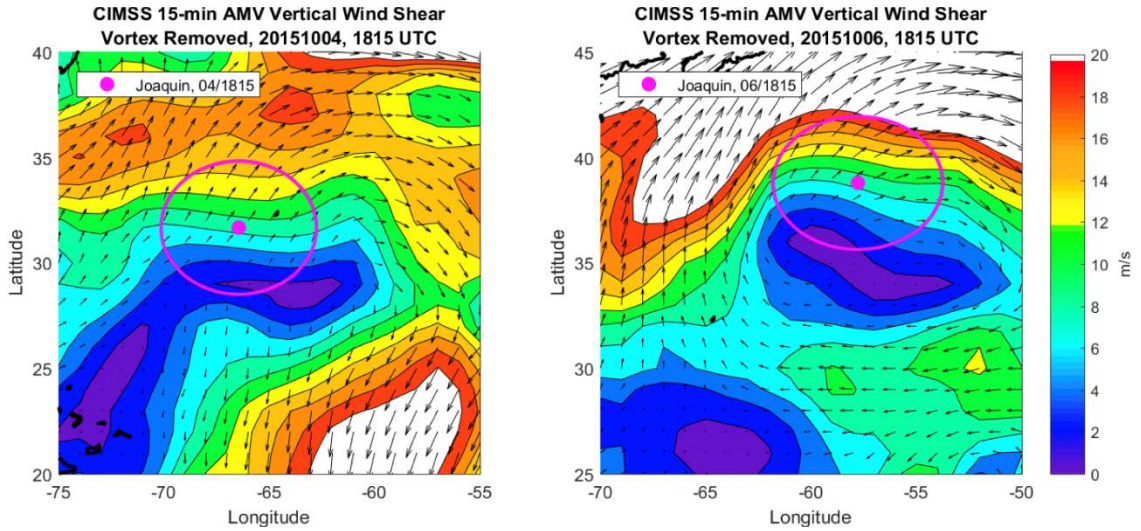

Horizontal plots of the VWS-C vectors relative to the position of Joaquin (magenta dot) during the interruption of rapid decay. The VWS-C values in Figure 9 and Table 2 are averaged over the circle with a radius of 350 km (left) 1815 UTC 4 October and (right) 1815 UTC 6 October.

Figure 22. CIMSS VWS plots during interrupted rapid decay period

As discussed in earlier segments, the VWS-C magnitudes were not uniform throughout the 350 km radius circle at 1815 UTC 4 October (Figure 22, left) as well as at 1815 UTC 6 October (Figure 22, right) during the interrupted decay. Specifically, Joaquin was within a large north-south gradient in VWS-C. At 1815 UTC 4 October (Figure 22, left), there is an area to the north-northeast of the storm center with VWS-C ~18 m s^{-1} and an area to the south-southeast with VWS-C < 4 m s^{-1}. The outflow from Joaquin would also be toward the north-northeast at this time (Figure 23, left), the asymmetrical VWS-C in Figure 22 (left) may be associated with an increase in the outflow, and thus aiding in a slight intensification of Joaquin rather than the expected decay in larger VWS-C. A similar VWS-C pattern existed later in Segment D at 1815 UTC 6 October, except the VWS-C magnitudes north-northeast of the storm are > 20 m s^{-1} in the direction of the outflow (Figure 23, right). Furthermore, the position of the short-wave trough to the west of the center is generally regarded as favorable to intensification. As indicated in the satellite

imagery in Figure 23 (right), Joaquin is undergoing extratropical transition at this time. Interestingly, the short-term re-intensification on 6 October is larger than on 4 October (Figure 9), which suggests again the importance of the asymmetrical VWS-C pattern to intensity change prediction. In summary, there appears to be a connection between the direction differences between the storm heading and the VWS heading, as well as the positions of large VWS-C gradients relative to Joaquin that lead the short re-intensification periods following the interrupted rapid decay of Joaquin described in Elsberry et al. (2018).

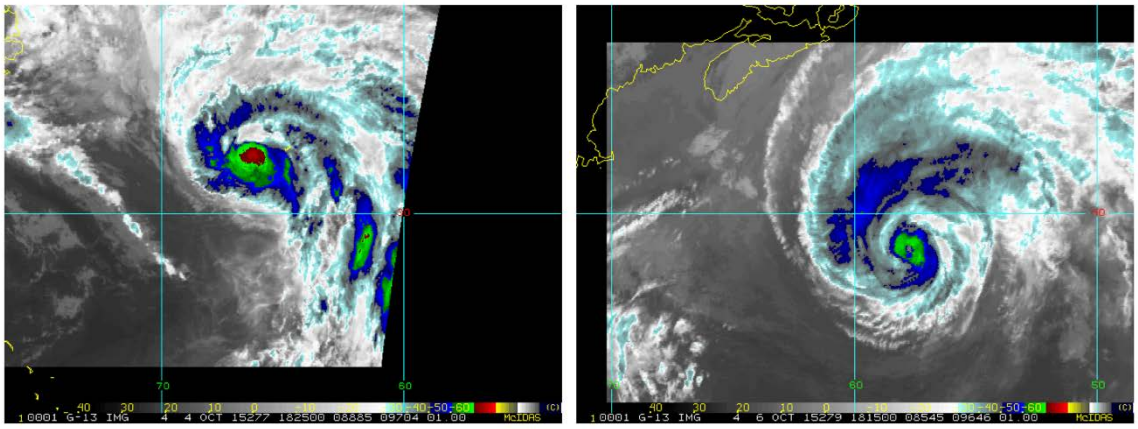

Remapped infrared imagery (~11 μm) at 4 km resolution taken from geostationary satellites GOES-East at (left) 1825 UTC 4 October 2015 and (right) 1815 UTC 6 October that correspond to horizontal VWS-C plots in Figure 22.

Figure 23. Enhanced IR satellite images of Joaquin at 1825 UTC 4 October and 1815 UTC 6 October. Source: NOAA Satellites and Information, Regional and Mesoscale Meteorology Branch (RAMMB) (Accessed: 10 April 2019).

THIS PAGE INTENTIONALLY LEFT BLANK

IV. SUMMARY AND CONCLUSIONS

A. SUMMARY

In summary, this thesis has used two special CIMSS datasets that are higher resolution (spatially and temporally) VWSs than the 6 h VWS-S, and the 30 min SATCON intensity estimates rather than the 6 h NHC best-track intensities, which are the most commonly used for analysis of TCs. Analysis of the SATCON dataset with observations every 30 min has demonstrated nuances in intensity changes of Joaquin that cannot be resolved when only analyzing values at the 6 h synoptic times. Likewise, the VWS-C dataset demonstrated that there were multiple times during the Joaquin life cycle when the VWS-C magnitudes and directions changed between 6 h synoptic times. For example, the VWS-C changed direction three times over less than 12 h during Segment B, which would not have been possible to resolve with only 6 h observations. Since the new-generation GOES satellites described in Chapter II have the capability for full-disk imagery at a 10-min temporal resolution, the Navy should use this capability to better model the environmental VWS and its impacts on the vertical structure of TCs.

A better understanding of the environmental factors that contributed to Joaquin's intensification and decay was reached by correlating the SATCON intensity changes with the 15-min VWS-C datasets. In particular, the SATCON / VWS-C correlation coefficient was much higher than the correlation coefficient obtained between the NHC best-track intensities versus the 6 h SHIPS VWSs. Correlations between the VWS-C and the SATCON datasets were demonstrated by examining different intensity change events and segments during Joaquin's life cycle, which led to much higher correlation coefficients (Table 2) than by calculating linear correlation coefficients over the entire life cycle of Joaquin.

The term "moderate" VWS-C has been used in Figure 8 and Table 2 to compare VWS-C with the intensity changes of Joaquin. In this thesis, a value of around 8 m s^{-1} was defined as "moderate." It was demonstrated that even small changes above and below the 8 m s^{-1} value were associated with both the intensification periods and the rapid decay of

Joaquin. In Segment A, a small VWS-C increment above 8 m s^{-1} was sufficient to delay intensification of a tropical depression to become a tropical storm. However, Joaquin underwent the first RI when only a small VWS-C decrease to near 8 m s^{-1} occurred. Once that RI occurred, continued VWS-C values of ~8 m s^{-1} during an extended period during Segment B with intensity changes of 5–10 kt per 6 h (i.e., rates of 30 - 60 kt per day according to SATCON estimates, which are not restricted to the normal practice of digitized intensities at 5 kt increments). In the counter-intuitive Event II, no lower bound on "moderate VWS-C" could be established as to when intensification would normally be expected, because intensity decreases were actually observed even though VWS-C became as small as ~4 m s^{-1}. Indeed, such small VWS values would normally be expected to be associated with rapid intensification rather than decreasing intensities. Subsequently, the second Joaquin RI began when the VWS-C had only increased to the representative moderate VWS values of 7 and 8 m s^{-1}. Perhaps the most counter-intuitive event was that the peak 6-h intensity change of 15 kt during the second RI was concurrent with a 6 h average VWS-C of 13 m s^{-1}, which would normally be expected to be associated with a rapid intensity decrease. Then the extreme decay rates of 5–10 kt per 6 h during the Event IV ended shortly after 2100 UTC 4 October when the VWS-C had decreased only into the moderate range at 8 m s^{-1}. According to the SATCON intensity estimates, continued decay after 0000 UTC 5 October was followed by small intensifications or decays when the VWS-C continued in the moderate range. In conclusion, this Joaquin case well illustrates that the relationship between environmental VWS and tropical cyclone intensity change is not linear -- rather this relationship can be highly nonlinear.

Another counter-intuitive aspect of Event II was when the intensity of Joaquin was decreasing when the VWS-C had decreased to ~4 m s^{-1}. A conceptual model was proposed (Figure 16) of how the ocean cooling during the southwestward path of Joaquin may explain the decay when the VWS-C was so small. A notch in the deep convection over the ocean-cooled air results as the warm, moist inflow is displaced well to the east of the center, and thus the strongest deep convection was well to the southeast rather than over the center. Consequently, the shift of the deep convection (and strong diabatic heating) may also explain the steering flow changes that led to the Joaquin track reversal. Although the

RAMMB OHC plots indicate some decreases in OHC in relation to the Joaquin track, other sea-surface temperature or OHC analyses are needed to confirm the ocean-cooling magnitudes and locations. Then, COAMPS-TC and NAVGEM forecasts need to be made to demonstrate whether the ocean cooling may have led to asymmetric deep convection that would account for the decay of Joaquin in low VWS and also whether that asymmetric deep convection could explain steering flow changes that led to the Joaquin track reversal.

B. FUTURE WORK

The long-term objective will be to demonstrate that the inclusion of these high temporal resolution AMVs will improve both the COAMPS-TC and (especially) the NAVGEM forecasts of the track reversal of Hurricane Joaquin. This observational study of the intensity changes prior to, during, and after the track reversal Joaquin has led to a conceptual model of the ocean cooling as an additional environmental factor. Model sensitivity studies are needed to demonstrate if (and how) the OHC distribution and ocean cooling impacts on Joaquin may have significantly contributed to the RI events and the track reversal.

Therefore, a three-part study is recommended to systematically examine the impacts of both the AMV-based environmental VWS-C and the ocean cooling. In the first approach, the ocean cooling might be predicted with a simple one-dimensional ocean model. The predicted SSTs along the southwestward path of Joaquin should be an improvement on the OHC changes analyzed in this thesis. However, utilizing a fully coupled COAMPS-TC would be a better approach. In order to do this, the same 15-min interval AMVs that were the basic input to the VWS-C product should be assimilated via the Four-dimensional COAMPS Dynamic Initialization (FCDI) technique into three-dimensional analyses that are not only the initial conditions for the next COAMPS-TC forecast but are also upscaled into the NAVGEM model. The primary objectives are to more accurately predict the upper ocean structure along the southwestward path that would impact Joaquin's intensity decrease after passing around the bottom of the track loop. If the track forecast is also improved, then the hypothesis can also be tested that the asymmetric deep convection relative to the ocean cooled air was a contributing factor to

the track reversal. The next test would be to input the new-generation optical flow AMV dataset from CIMSS at the upper levels of the atmosphere to more accurately predict the convergence and divergence aloft in Joaquin. The third recommended step would then be to combine the ocean cooling effects and the new generation AMVs into the model to more accurately predict the physical processes at the bottom and at the top of Joaquin, and more accurately predict the correct asymmetric diabatic heating. This third test should contribute to the largest forecast improvements of the track and the intensity changes of Joaquin.

In summary, this thesis has defended the environmental factors that are considered to be most important to predict the track reversal of Joaquin in a global model such as NAVGEM. The key hypothesis arising from this observational study is that the transition to highly asymmetric deep convection (and thus diabatic heating profile in the vertical) relative to the center will contribute to Joaquin having a northeastward track after striking the Bahamas. Whereas the lower-tropospheric Joaquin circulation will move along the west side of the ocean-cooled air, the upper-tropospheric warm core diabatic heating is hypothesized to switch to the east of that region when the notch in the deep convection is present, and thus will tend to lower the surface pressures to the southeast of the ocean-cooled air. The lower pressures to the southeast are hypothesized to shift the steering flow to have a more northeastward component after Joaquin moves poleward along the ocean-cooled region. While such a NAVGEM modeling study will be challenging, a success in modeling the Joaquin track reversal would open new opportunities to more accurately predict tropical cyclones that threaten Naval assets and personnel.

LIST OF REFERENCES

Berg, R. L., 2016: National Hurricane Center Tropical Cyclone Report: Hurricane Joaquin (AL112015), 36 pp, https://www.nhc.noaa.gov/data/tcr/AL112015_Joaquin.pdf.

Doyle, J., and Coauthors, 2017: A view of tropical cyclones from above: The Tropical Cyclone Intensity experiment. *Bull. Amer. Meteor. Soc.*, **16**, 2113–2134, DOI: https://doi.org/10.1175/BAMS-D-16-0055.1.

Elsberry, R. L., and R. Jeffries, 1996: Vertical wind shear influences on tropical cyclone formation and intensification during TCM-92 and TCM-93. *Mon. Wea. Rev.*, **124**, 1374–1387.

Elsberry, R. L., and M. S. Park, 2017: Comments on "Multiscale structure and evolution of Hurricane Earl (2010) during rapid intensification." *Mon. Wea. Rev.*, **145**, 1565–1571, DOI: https://doi.org/10.1175/MWR-D-16-0301.1.

Elsberry, R. L., E. Hendricks, C. Velden, M. Bell, M. Peng, E. Casas, and Q. Zhao, 2018: Demonstration with special TCI-15 datasets of potential impacts of new-generation satellite atmospheric motion vectors on navy regional and global models. *Wea. Forecasting*, **33**, 1617-1637, DOI: https://doi.org/10.1175/WAF-D-17-0168.1.

Gallian, G., and C. Velden, 2002: Environmental vertical wind shear and tropical cyclone intensity change utilizing enhanced satellite derived wind information. Preprints, American Meteorological Society, 25th Hurricane and Tropical Meteorology conference, San Diego, CA, 172–173.

Griffith, Paul C., 2015: ABI delivers significantly increased capabilities over current imagers. ITT Space Systems Division, Accessed 5 October 2018, https://www.goesr.gov/downloads/GOES/20Users/27/20Conference/20IV/Complete/20Posters/GUC4_poster_Griffith.pdf.

Hendricks, E. A., M. Peng, B. Fu, and T. Li, 2010: Quantifying environmental control on tropical cyclone intensity change. *Mon. Wea. Rev.*, **138**, 3243-3271.

Hendricks, E., R. L. Elsberry, C. S. Velden, A. Jorgensen, M. S. Jordan, and R. Creasey, 2018: Environmental factors and internal processes contributing to interrupted rapid decay of Hurricane Joaquin (2015). *Wea. Forecasting*, **33**, 1251–1262, DOI: https://doi.org/10.1175/WAF-D-17-0190.1.

Hogan, P., and Coauthors, 2015: Status and future of global and regional ocean prediction systems. *J. of Oper. Oceanogr.*, **8: Sup 2**, 201–220, DOI: 10.1080/1755876X.2015.1049892.

Jorgenson, A., 2017: Factors contributing to the interrupted decay of Hurricane Joaquin (2015) in a moderate vertical wind shear environment. M.S. thesis, Dept. of Meteorology, Naval Postgraduate School, 97 pp.

National Transportation Safety Board, 2017: Sinking of U.S. Cargo Vessel SS *El Faro*, Atlantic Ocean, northeast of Acklins and Crooked Island, Bahamas, October 1, 2015. Marine Accident, 300 pp, https://www.ntsb.gov/investigations/accidentreports/reports/mar1701.pdf.

Report NTSB/MAR-17/01. Washington, DC. NOAA Office of Satellite and Product Operations, RAMMB, 2019: Tropical Cyclone Archive: Hurricane Joaquin (2105). Accessed: 21 February 2019, http://rammb.cira.colostate.edu.

University of Wisconsin, 2019: CIMSS SATCON. Accessed: 28 February 2019, tropic.ssec.wisc.edu/misc/satcon/info.html.

Velden, C. S., and Coauthors, 2005: Recent innovations in deriving tropospheric winds from meteorological satellites. *Bull. Amer. Meteor. Soc.,* **86**, 205–223, DOI: https://doi.org/10.1175/BAMS-86-2-205.

Velden, C. S., and J. Sears, 2014: Computing deep-tropospheric vertical wind shear analyses for tropical cyclone application: Does the methodology matter? *Wea. Forecasting,* **29**, 1169–1180. DOI: https://doi.org/10.1175/WAF-D-13-00147.1.

INITIAL DISTRIBUTION LIST

1. Defense Technical Information Center
   Ft. Belvoir, Virginia

2. Dudley Knox Library
   Naval Postgraduate School
   Monterey, California